PAPER IV

Darnis G, Hobbs L, Geoffroy M, Grenvald JC, Renaud P, Berge J, Cottier F, Kristiansen S, Daase M, Søreide J, Wold A, Morata N, Gabrielsen TM (accepted)

From polar night to midnight sun: diel vertical migration, metabolism and biogeochemical role of zooplankton in a high Arctic fjord (Kongsfjorden, Svalbard)

Limnology and Oceanography

From polar night to midnight sun: diel vertical migration, metabolism and biogeochemical role of zooplankton in a high Arctic fjord (Kongsfjorden, Svalbard)

G. Darnis[1*], L. Hobbs[2], M. Geoffroy[3,4], J. C. Grenvald[5], P. E. Renaud[1,5], J. Berge[4,5], F. Cottier[2,4], S. Kristiansen[4], M. Daase[4], J. Søreide[5], A. Wold[6], N. Morata[1], T. Gabrielsen[5]

[1] Akvaplan-niva. Fram Centre for Climate and the Environment, N-9296 Tromsø, Norway.
[2] Scottish Association for Marine Science, Oban, United Kingdom, PA37 1QA.
[3] Université Laval, Pavillon Alexandre-Vachon, 1045, avenue de la Médecine, Québec (QC) G1V 0A6, Canada.
[4] Faculty of Biosciences, Fisheries and Economics, UiT The Arctic University of Norway, N-9037 Tromsø, Norway.
[5] University Centre in Svalbard, Pb 156, N-9171 Longyearbyen, Norway.
[6] Norwegian Polar Institute, 9296 Tromsø, Norway.

[*] Corresponding author: Gerald.Darnis@akvaplan.niva .no

Running title: Zooplankton migration and biogeochemical fluxes

Keywords: Biological pump, Carbon flux, Krill Respiration, Excretion

Abstract

Zooplankton vertical migration enhances the efficiency of the ocean biological pump by translocating carbon (C) and nitrogen (N) below the mixed layer through respiration and excretion at depth. We measured C and N active transport due to diel vertical migration (DVM) in a Svalbard fjord at 79°N. Multifrequency analysis of backscatter data from an Acoustic Zooplankton Fish Profiler moored from January to September 2014, combined with plankton net data, showed that *Thysanoessa* spp. euphausiids made up >90% of the diel migrant biomass. Classical synchronous DVM occurred before and after the phytoplankton bloom, leading to a mismatch with intensive primary production during the midnight sun. Zooplankton DVM resulted in C respiration of 0.9 g m^{-2} and ammonium excretion of 0.18 g N m^{-2} below 82 m depth between February and April, and 0.2 g C m^{-2} and 0.04 g N m^{-2} from 11 August to 9 September, representing >25% and >33% of sinking flux of particulate organic carbon and nitrogen, respectively. Such contribution of DVM active transport to the biological pump in this high-Arctic location is consistent with previous measurements in several equatorial to subarctic oceanic systems of the World Ocean. Climate warming is expected to result in tighter coupling between DVM and bloom periods, stronger stratification of the Barents Sea, and northward advection of boreal euphausiids. This may increase the role of DVM in the functioning of the biological pump on the Atlantic side of the Arctic Ocean, particularly where euphausiids are or will be prevalent in the zooplankton community.

Introduction

The World Ocean plays a critical role in the mitigation of the planetary greenhouse effect due to CO_2 by absorbing about one third of the anthropogenic emissions of carbon to the atmosphere (Marinov and Sarmiento 2004). The oceanic uptake of CO_2 is regulated by physical and chemical processes, referred to as the "solubility pump", and a complex set of biological processes known as the "biological pump" (Ducklow et al. 2001). The mechanics of the latter involve the fixation of inorganic carbon by phytoplankton photosynthesis in the photic layer and subsequent vertical translocation of pelagic new primary production, either by sinking (passive or sinking flux) or transport (active flux), to depth below a pycnocline (Longhurst and Harrison 1988; Steinberg et al. 2000; Steinberg et al. 2002).

In the temperate and tropical ocean, extensive diel vertical migration (DVM) of zooplankton and micronekton has been shown to play a significant role in the vertical flux of particulate and dissolved organic matter (Longhurst et al. 1990; Steinberg et al. 2002; Takahashi et al. 2009). Active transport can represent up to 70% and 82% of the sinking fluxes of particulate organic carbon (POC), and nitrogen (PON), respectively (Dam et al. 1995). Typically, herbivorous zooplankton feed in the epipelagic layer at night and migrate to depth before dawn to avoid predation by visual predators (Brierley 2014). There they release carbon and nitrogen during egestion, and as CO_2 and NH_4^+ through respiration and excretion (Bronk and Steinberg 2008; Steinberg et al. 2008).

In Arctic ecosystems, the high seasonality in light climate, shifting between the "polar night" (when the sun remains below the horizon) and "midnight sun" (when the sun does not set for extended periods) seasons makes zooplankton DVM responses more complex than at lower

latitudes (Last et al. 2016; Ringelberg 2010). The rapid changes in day-night cycle and other environmental factors affect timing, synchrony and vertical range of migration (Berge et al. 2014; Fischer and Visbeck 1993), which in turn influence the transport potential over the year. In such a variable light environment, snapshot sampling during scientific cruises limits the assessment of the consequences of zooplankton DVM. However, studies using multi-month time-series of acoustic data from moored instruments have shed light on the seasonal patterns of DVM. Acoustic Doppler Current Profilers (ADCPs) have recorded periods where zooplankton behavior resembles classical DVM, when the relative rate of change in irradiance is sufficient to trigger synchronous movements of zooplankton in winter-spring and autumn. The data have also suggested unsynchronized (individual) vertical movements under the continuous illumination of the Arctic summer when algal food is usually plentiful in the surface layer (Berge et al. 2009; Cottier et al. 2006; Wallace et al. 2010). Plankton-net data, sometimes combined with acoustic data, have shown that euphausiids, hyperiid amphipods, large *Calanus* and *Metridia* copepods, chaetognaths and ctenophores are the main diel migrants in Arctic waters, their relative importance fluctuating with seasons and locations (Berge et al. 2014; Daase et al. 2008; Fischer and Visbeck 1993; Fortier et al. 2001).

One study based on a 10-month analysis of zooplankton in the southeastern Beaufort Sea revealed the importance of seasonal vertical migration (SVM) for carbon budgets in Arctic systems (Darnis and Fortier 2012). Carbon export below 200 m depth, mediated by large seasonal migrants such as the Arctic copepods *Calanus hyperboreus* and *C. glacialis* that overwinter at depth, was found to be of the same magnitude as the annual sinking POC flux measured by sediment traps. The impacts of both the well-known DVM taking place during the lighted season (Cottier et al. 2006; Wallace et al. 2010) and the recently discovered DVM during polar night

(Berge et al. 2009; Wallace et al. 2010), however, have not been estimated. It is likely that ongoing DVM by some components of the community during winter will add to the proportion of vertical flux during this season accounted for by SVM. The consequences of DVM for the biological pump around the time of maximum new production are difficult to predict, however. This information is needed if we are to forecast the response of the Arctic marine ecosystem to the rapid warming of its waters and potential alteration of timing of ecological processes and the faunal assemblages present (Ardyna et al. 2014).

Here, we document the effect of synchronous DVM on the export to depth of carbon and nitrogen, using a 7-month time series of acoustic data collected with a moored Acoustic Zooplankton Fish Profiler (AZFP) in combination with plankton-net sampling in a high-Arctic Svalbard fjord, Kongsfjorden. In particular, we measure remineralization of carbon through respiration and excretion of ammonium at depth and assess the importance of the active transport relative to other fluxes.

Methods

Environmental setting of the study area

Sampling was carried out at or in the vicinity of station KB3 (78°57'N, 11°56'E, ca. 320 m depth) in the outer basin of Kongsfjorden (Fig. 1). Located on the west coast of Spitsbergen, Svalbard archipelago, Kongsfjorden is a wide glacial fjord consisting of two main basins separated by a 30 m-deep sill (Svendsen et al. 2002). Three large tidewater glaciers calve into the relatively shallow inner basin (<80 m depth), providing the main source of freshwater to the fjord (Cottier et al. 2005). Seaward, a submarine glacial trench (Kongsfjordrenna) connects the deeper (<400 m depth) outer basin of Kongsfjorden to the West Spitsbergen Shelf and allows relatively free

118 water-mass exchange across the shelf-fjord boundary. The fjord is therefore largely influenced by
119 advection of both warm, saline Atlantic Water from the West Spitsbergen Current and colder,
120 fresher Arctic water originating from the more coastal East Spitsbergen Current (Fig. 1) (Cottier
121 et al. 2005; Svendsen et al. 2002). The Kongsfjorden zooplankton assemblage, a mixture of
122 boreo-Atlantic and Arctic species, reflects the dual influence of these water masses (Basedow et
123 al. 2004; Kwasniewski et al. 2003; Willis et al. 2006). The fjord has remained essentially ice-free
124 since a major inflow of Atlantic Water during the winter of 2005-2006 (Cottier et al. 2007). In
125 winter, the entire water column is homogeneous (Fig. 2) but a strong pycnocline forms during the
126 summer months, as a result of strong freshwater discharge due to glacial and snow melt (Cottier
127 et al. 2010).
128
129 The light regime in Kongsfjorden, at 79^{o}N, is characteristic of high latitude regions with the sun
130 remaining more than 6^{o} below the horizon from 10 November to 1 February, the so-called "polar
131 night" period (Berge et al. 2015). In contrast, the "midnight sun" period extends from 18 April to
132 23 August when the sun does not set below horizon.
133
134 Timing of the spring phytoplankton bloom in Kongsfjorden is variable and dependent upon
135 physical factors, such as light levels, occurrence of sea ice inside and outside the fjord, and
136 mixing processes, (Hegseth and Tverberg 2013). Usually, the spring bloom takes place between
137 mid-April and late May (Hegseth and Tverberg 2013; Hodal et al. 2012; Seuthe et al. 2011).
138
139 ***Acoustic sampling and data analysis***
140 Several moorings were deployed over the course of 2013-2014 at a short distance from sampling
141 station KB3 (Fig. 1). The instruments fitted on the moorings are detailed in Table 1. On one of

142 the moorings, an upward-looking Acoustic Zooplankton Fish Profiler^{TM} (AZFP; ASL
143 Environmental Science Inc., Victoria, Canada) continuously recorded hydroacoustic data at 125,
144 200, 455, and 769 kHz from 17 January to 9 September 2014. Since the 769 kHz transducer only
145 insonified a water layer of a few meters above the instrument, data from only the three lower
146 frequencies were considered in this study. The AZFP was moored at 84 m within a stainless steel
147 frame supported by floats. To limit the backscatter from other moored instruments located higher
148 on the mooring line, the AZFP was mounted with an 8º angle relative to the vertical mooring line.
149 The vertical angle, the pitch and roll of the AZFP were taken into account in the internal beam-
150 mapping algorithm of the AZFP to assign real depths to mean volume backscattering strength (Sv
151 in dB re 1 m^{-1}) and target strength (TS in dB re 1 m^{-2}) values. Vertical resolution varied from 23.6
152 cm at 455 kHz to 98.4 cm at 125 kHz. The pulse duration and nominal beam angle also varied
153 with the frequency (Table S1). Source level was 210 dB (re 1µPa at 1m) and ping rate was 1
154 ping·10 sec^{-1} (0.1 Hz) from 17 to 22 January and 0.05 Hz thereafter. The AZFP was calibrated
155 by the manufacturer (± 1 dB) prior to deployment (ASL 2014).
156
157 Acoustic data were processed with EchoView® 6.0. Bad pings, the backscatter from the sediment
158 trap, the top two meters of the water column and the first two meters nearest to the AZFP were
159 excluded from the analysis. Strong echoes typical of fish schools (Fig. S1) were also removed
160 from the echograms to keep only the signal from zooplankton. The monthly echogram at each
161 frequency was divided into 1-meter vertical by 5-minutes horizontal echo-integration cells and
162 mean Sv within each cell was exported.
163
164 Scattering models can be used to predict the acoustic response of scatterers to specific
165 frequencies (Stanton et al. 1998). This response varies between types of zooplankton (or

functional groups) due to changes in body shape, size, orientation, and the contrast in density and sound speed between scatterers and the surrounding water (Kristensen and Dalen 1986; Lawson et al. 2004). Net samples from Kongsfjorden in January 2014 showed the most numerically dominant functional groups to be copepods, euphausiids, and chaetognaths. These three groups can all be modeled as fluid-like weak scatterers (Stanton and Chu 2000) using the Distorted Wave Born Approximation approach (Stanton et al. 1998). Scattering models were fitted for each functional group using a range of sizes (Table S2) and specific orientation angles for copepods (Benfield et al. 2000), euphausiids (Chu et al. 1993) and chaetognaths (Fredrika Norrbin; unpublished Video Plankton Recorder data from Kongsfjorden), at the three frequencies of the AZFP. These models demonstrated that euphausiids have a frequency response of $Sv_{125kHz} > Sv_{200kHz} < Sv_{455kHz}$; copepods of $Sv_{125kHz} < Sv_{200kHz} < Sv_{455kHz}$; and chaetognaths $Sv_{125kHz} < Sv_{200kHz} > Sv_{455kHz}$. Using these differences in the frequency responses, each echo-integration cell was partitioned into one of the three functional groups, which was assumed to be dominant within that given cell.

Mean Target Strength (TS) for each functional group was then estimated based on the randomly oriented fluid bent cylinder model (Stanton et al. 1994). The average dry weight *W* of individual euphausiids and copepods was estimated from measurements of individuals made on a microbalance whereas the *W* of chaetognaths was estimated using a length-dry weight relationship established for *Parasagitta elegans* (Welch et al. 1996) (Table S2). Mean dry biomass (mg m^{-3}) within each echo-integration cell associated with euphausiids (Equation 1), copepods (Equation 2), or chaetognaths (Equation 3) was calculated following Parker-Stetter et al. (2009):

$$Biomass_{euphausiids} = \left(\frac{s_{v_{125kHz}}}{\sigma_{bs_{euphausiids}}}\right) \cdot W_{euphausiids} \quad (1)$$

$$Biomass_{copepod} = \left(\frac{s_{v_{455kHz}}}{\sigma_{bs_{copepodss}}}\right) \cdot W_{copepods} \quad (2)$$

$$Biomass_{chaetognaths} = \left(\frac{s_{v_{200kHz}}}{\sigma_{bs_{chaetognaths}}}\right) \cdot W_{chaetognaths} \quad (3)$$

Where s_v is the linear volume backscattering strength (m^2 m^{-3}), σ_{bs} is the expected backscattering cross-section of an element of the zooplankton group (m^{-2}), and and W is the average dry weight (mg) . The biomass of each zooplankton group was integrated in the top 2-40 (above the trap) and 2-82 m layers and averaged for each month during the day and the night hours. Day was defined as the time-interval of minimum backscatter in the targeted water layer around local midday measured on the echogram at 125 kHz of the AZFP (Fig. S2), whereas night was the period of higher backscatter during the remainder of the 24-h cycle. Dry biomass was converted to carbon content using the C:W factor of 0.5189, 0.5366 and 0.3844 for euphausiids (i.e. *Thysanoessa inermis*), large copepods and chaetognaths (i.e. *Parasagitta elegans*), respectively (Ikeda and Skjoldal 1989).

To gain insight into the zooplankton DVM patterns beyond the period sampled with the AZFP (until 9 September), additional acoustic data were obtained during a short-term mooring deployment close to the autumn equinox (23-25 September). The mooring was equipped with two 307-kHz RDI ADCPs, one upward-looking at 95 m, the other downward-looking at 96 m. In

addition a Parflux 21-cup sediment trap was positioned at 65 m to intercept sinking particles and zooplankton swimmers (Table 1). The ADCPs measured the mean echo strength from ensembles of 60 pings at a rate of 1 ping s^{-1} in 22 depth layers (bins of 4 m). The raw echo intensity data were converted to a measure of absolute volume backscatter (Sv, in dB) (Berge et al. 2014). The ADCPs would detect zooplankton of the size of medium to large *Calanus* copepodite stages (>5 mm of prosome length) and larger.

A Seapoint fluorometer and PAR sensor, both mounted at 37 m depth on an adjacent mooring, provided raw fluorescence and Photosynthetic Active Radiation data in the vicinity of station KB3 from 5 October 2013 to 9 September 2014.

Ship-based sampling and taxonomic analysis

Net sampling for macro- and meso-zooplankton was carried out at station KB3 using R/V *Helmer Hanssen* from 16 to 20 January and 23 to 27 September 2014. Additional mesozooplankton samples were taken between 12 and 14 May, using the workboat *Teisten*, and on 23 July using R/V *Lance*. Macrozooplankton was sampled as close as possible to local midday and midnight by trawling obliquely from 30 m depth to the surface at 2 knots for approximately 5-10 minutes with a Methot-Isaac-Kidd (MIK) ring net (3.15 m^2 aperture, 13-m long net with 1500 µm mesh size and a 500 µm mesh in the last meter), fitted with a 10-L cod end and equipped with a Hydrobios flowmeter at the center of the ring. Upon retrieval, the zooplankton samples were subdivided and 2/3 to 3/4 of the cod end was fixed in a borax-buffered seawater solution of 4% formaldehyde for taxonomic identification. Nine and four MIK net deployments were done in January and September, respectively.

236 Mesozooplankton was sampled around midday and midnight, using a Hydro-Bios multiple
237 plankton sampler Midi-MultiNet (0.25 m^2 aperture, 5 nets of 200-µm mesh) hauled vertically at
238 0.5 m min^{-1}. The sample depths were 320-200, 200-100, 100-50, 50-20, and 20-0 m depth. In
239 May, successive deployments of a KC Denmark WP2 net (0.25 m^2 aperture, 200-µm mesh) with
240 a closing system were done instead of the MultiNet sampling, and the deepest stratum sampled
241 reached 300 m depth. No replicate sampling of each depth stratum was performed. Upon
242 collection, the content of the cod ends was preserved in seawater solution of 4% hexamethylen-
243 buffered formaldehyde for taxonomic identification. Four Multinet deployments were performed
244 in January, three in May, one in July, and four in September. CTD (Seabird SBE 911) casts
245 through the water column were carried out immediately before or after net deployments to collect
246 profiles of temperature, salinity and fluorescence.
247
248 In January, May and September, additional MIK and MultiNet/WP2 casts were carried out at
249 station KB3 to catch live zooplankton for respiration, ammonium excretion and biomass
250 measurements. The sampling using a WP2 or WP3 (1 m^2 aperture, 1000-µm mesh) net was
251 performed on the Svalbard shelf from 18 to 28 May for mesozooplankton respiration
252 measurement onboard *Helmer Hanssen*. Each net of the samplers was fitted with a rigid cod end
253 with filtration apertures at the top of the cylinder to keep the animals in sufficient water until
254 collection. Upon retrieval, each sample was diluted in cold filtered (0.2-0.7 µm GF/F) seawater
255 (FSW) and any large jellyfish were removed. Other macrozooplankton such as amphipods,
256 euphausiids, and *Clione limacina* were also removed from the samples collected with the
257 MultiNet/WP2 to avoid predation and stress on the mesozooplankton size class. The live samples
258 were kept in the dark in a temperature-controlled room set at close to *in situ* temperature (1-4^{o}C)
259 until further treatment.

In the laboratory, known aliquots (up to 1/8) were taken from the MIK formalin-preserved macrozooplankton samples and all non-copepod organisms were counted and identified to species level under a stereomicroscope before measuring their total body length. Samples from the MultiNet casts were size-fractionated on a 1000-µm sieve and re-suspended in distilled water. Successive known aliquots were taken from the 200-1000-µm fraction with a 5-mL large tip (>5 mm diameter) automatic pipette until 300 organisms were counted and identified to developmental stage and species, or to the lowest possible taxonomic level, under a stereomicroscope. The >1000-µm fraction was analysed in its entirety. Prosome length of the *Calanus* copepodites was measured in both size-fractions.

Zooplankton biomass, respiration and ammonium excretion

Intact and active individuals of dominant macrozooplankton taxa, essentially *Thysanoessa* spp., *Themisto abyssorum* and *Themisto libellula*, were rapidly sorted from the MIK live samples. A known subsample of each of the live samples collected with the Multinet/WP2 was poured into a funnel fitted with a 1000-µm sieve inside and a gate valve to obtain two mesozooplankton size classes for incubation. The >1000-µm fraction was retained in the top part of the device in a sufficient volume of water while the 200-1000 µm small zooplankton was gently evacuated through the sieve through successive washes with cold oxygenated, filtered seawater. A sufficient number of macrozooplankton animals (1-10 depending on size and volume of incubation bottle) and each mesozooplankton size class were gently introduced in separate airtight glass bottles (110-280 mL capacity), which were thereafter filled with cold oxygenated filtered seawater and capped. Control bottles without zooplankton were made in triplicates for each experimental setup. Oxygen concentration was measured by optode respirometry with a 4-channel respirometer

(Oxy-4 Mini, PreSens Precision Sensing GmbH, Regensburg Germany) every 0.5-2 hours for 8-12 h. Respiration rates were calculated by determining the slope of the decrease of oxygen over time and subtracting the mean value for the controls. Oxygen consumption rates were transformed to respiratory carbon using a respiratory quotient of 0.75 in January, assuming a winter metabolism mainly by lipid reserves (Ingvarsdóttir et al. 1999), and 0.97 from May onward with a metabolism primarily based on proteins (Gnaiger 1983).

Zooplankton ammonium (NH_4^+) excretion rate was estimated from the same incubations used for respiration and calculated as the difference in NH_4^+ concentration between incubation bottles and animal-free control bottles at the end of the experiment divided by the duration of incubation to obtain an hourly rate. In January, ammonium concentration was measured onboard immediately after collection while, in September, the water samples were preserved in acid-cleaned 125-mL polycarbonate bottles and immediately frozen. During the January and September fieldwork, triplicate samples of water were taken before the incubation for ammonium measurement. At termination of incubation, triplicate samples were retrieved from the incubation water. The ammonium samples were filtered through acid-washed Sartorius polycarbonate syringe filter holders equipped with pre-burned Whatman GF/C glass microfibre filters (6 hrs at 450^{o}C). The filter holders were rinsed with deionized Milli-Q water before use. NH_4-N concentration was analysed spectrofluorimetrically using a 5-cm cell following Solórzano (1969).

Right after the experiments organisms were carefully blotted on absorbent material and preserved in cryovials at -20^{o}C. In the laboratory, the frozen samples were transferred to pre-weighed plastic cups, dried in an oven at 60^{o}C for 48 h and then weighed on a microbalance (±1μg).

307 Carbon content (C) of each macro- and meso-zooplankton taxon was calculated from dry mass
308 (*W*) measurements, using the specific C-*W* relationship in Ikeda and Skjoldal (1989).
309
310 ***Active respiratory carbon and excretory nitrogen transport***
311 To study the seasonal variation in zooplankton DVM patterns (spatial extent and strength in
312 terms of biomass involved), and resulting active fluxes of carbon and nitrogen, the daily migrant
313 biomass *MB* (mg C m^{-2}) of euphausiids, copepods and chaetognaths was calculated. Monthly
314 averages of migrant biomass integrated from surface to depth (z) over the 7-month time series
315 were determined from equation (4):
316
317 $MB_z = \int_z$ night biomass-day biomass (4)
318
319 Transport out of the top 2-40 and 2-82 m depth strata was considered. The lower limit of the layer
320 (*z*) was set at 40 m depth for comparison of active transport with sinking flux measured with a
321 sediment trap at that depth whereas *z* at 82 m corresponds to the maximum depth sampled with
322 the AZFP.
323
324 The downward active transport at depth *z* was then calculated using equation (5):
325
326 $AF_z = MB \times RE \times T$ (5)
327
328 where *AF* is the active transport of carbon (mg C m^{-2} d^{-1}) or nitrogen (mg N m^{-2} d^{-1}) by migrant
329 zooplankton, *RE* is the specific hourly respiratory carbon loss (mg C mg C^{-1} h^{-1}) or ammonium

excretion (mg N mg C^{-1} h^{-1}), and *T* (h) is the time spent at depth during a 24-h cycle. *T* was measured from the AZFP echogram at 125 kHz.

To calculate daily rates of community respiration, excretion and active transport due to DVM averaged over each month of the time-series, hourly specific metabolic rates of the different taxa and size classes had to be interpolated by using the three snapshot measurements of hourly rates of January, May and late September to cover the whole study period. For mesozooplankton, we assumed that the size class >1000 μm largely dominated by large copepods was primarily responsible for the backscatter recorded by the AZFP, and applied their specific hourly metabolic rates in the calculations. Chaetognath metabolic rates were not measured due to the difficulty of collecting undamaged individuals for incubations. Thus, we used a specific respiration of 0.40 ± 1.06 μg C mg C^{-1} h^{-1} and excretion of 0.15 ± 0.12 μg N mg C^{-1} h^{-1}, measured by Ikeda and Skjoldal (1989) on *Parasagitta elegans*, the dominant chaetognath in Kongsfjorden.

Sinking flux of Particulate Organic Carbon and Nitrogen (POC/PON)

To compare our estimates of active transport of carbon and nitrogen below the 40 and 82 m depths with sinking fluxes of POC and PON, we analysed samples from sequential automated sediment traps (McLane PARFLUX Mark78H; 0.66 m^2 collecting area; 21-cups turntable) deployed on moorings in Kongsfjorden (Table 1). A sediment trap at 40 m depth on the same mooring as the AZFP intercepted sinking particles from 21 January to 3 April 2014 at a sampling frequency of 3.5 days per cup. A large volume of terrigenous matter clogged a sediment trap at 100 m depth soon after deployment in October 2013, preventing from using the sediment samples to quantify sinking fluxes in the annual cycle 2013-2014. Therefore, we used the 2012-2013 time series of sediment samples to quantify POC and PON sinking at 100 m depth, assuming a low

interannual variability in sinking fluxes outside of the bloom period.

Before deployment, the sample cups were filled with seawater filtered through Whatman GF/F 0.7 µm glass fiber filters, adjusted to 35 PSU with NaCl, and poisoned with formalin (2% v/v, sodium borate buffered). After recovery, zooplankton were removed from the samples using a dissecting microscope. Samples were then subdivided using a Motoda splitting box and filtered in triplicates through pre-weighed GF/F filters (25 mm diameter, 0.7 µm pore, pre-combusted for 4 h at 450^{o}C). Filters were dried for 12 h at 60^{o}C, weighed for dry weight and exposed to concentrated HCl fumes for 12 h to remove inorganic carbon. They were folded in tin cups that were then combusted in a EuroEA3022 elemental analyser for measurement of POC and PON.

Results

Synchronous DVM

The continuous echogram of the AZFP at 125 kHz allows for the tracking of vertical distribution of scatterers over the 7-month period from the polar night to the end of summer. DVM behavior was identified qualitatively as periods of time where a strong scattering layer characterized by a strong band of green/red was seen to oscillate at a daily frequency over a depth range greater than 30 m (Fig. 3a). A clearly visible synchronous DVM extending below 40 m started on 28 January (Fig. 3b). From then on the depth range of the DVM signal increased, reaching 82 m on 31 January. This winter DVM persisted until 10 April (a few days before the onset of midnight sun), after which sporadic synchronous vertical movements did not usually occur in phase with the 24-h light cycle. Synchronous DVM resumed on 11 August, first with weak sporadic migrations (not every day), that reached a regular 24-h period in early September (Fig. 3c). Thus, classical DVM behavior occurred outside of the main season of primary production, between late May and late

June in 2014 as shown by the fluorescence at 37 m depth (Fig. 3a). Strong echoes during the midnight sun in June and early July in the 2-82 m layer, indicative of strong zooplankton biomass but without evidence of classical DVM, coincided with this period of high biological production in the surface layer.

The echogram of the backscatter recorded by the ADCPs over three days in late September, two weeks after the end of the AZFP sampling, shows a strong DVM signal (Fig.4). At midnight, the bulk of the backscatter was concentrated in the upper 20 m, whereas it was located between 120 and 160 m at midday.

Time spent at depth during a 24-h cycle

Time spent by scatterers below 40 m and below 82 m during a daily cycle showed a very similar strong linear increase from the start of DVM in late January to its end in April (Fig. 5). From early March onward, the small difference between times spent below 40 m and below 82 m indicated that the downward/upward migrations were swift from surface to below the two depth limits. From January to early March, zooplankton spent most of a diel cycle above 40 m or 80 m depth, with time at depth <12 hours. Conversely, at the end of the late winter DVM period when there was more than 12 h of light per day, zooplankton were distributed below 82 m most of the day (>20 h). The same situation can be seen in late August and early September at the onset of the autumn synchronous DVM season.

Composition of the migratory community from plankton net data

Macrozooplankton biomass in the surface 0-30 m layer estimated from the plankton net hauls tended to be slightly lower at midday than at midnight in January (Fig. 6). However, the low

number of net deployments during each short cruise prevented the comparison of day and night zooplankton biomass for statistical differences. Extremely low biomass at midday at the surface compared to night was observed in September, indicating a strong DVM pattern. Euphausiids (mainly *Thysanoessa inermis*, *T. raschii* and *T. longicaudata*) represented 94 ± 4 % of the macrozooplankton biomass at day and night in January and 91 ± 1% at night in September, but only 9 ± 3% of the day biomass in September. Chaetognaths (mainly *Parasagitta elegans*) contributed 5 ± 4% to the macrozooplankton biomass in January whereas they contributed 6 ± 3% of the biomass at night and 56 ± 16% at day in September when the biomass was extremely low. Contribution of the very few *Themisto* spp. to macrozooplankton biomass was negligible in January (<0.01%) and low at night in September (<3%). These amphipods represented, however, 30% of the very low surface macrozooplankton biomass a noon in September.

Mesozooplankton biomass in the surface 0-50 m layer did not show any difference between midday and midnight in January and May (Fig. 6). The biomass was lowest in May and highest in July, with *Calanus* spp. (*C. finmarchicus* and *C. glacialis*) dominating the mesozooplankton assemblage. These taxa, together with *C. hyperboreus* and *Metridia longa*, represented 69, 68, 92 and 89% of the biomass at midday in January, May, July, and September, respectively, in the 0-50 m layer and 55 and 45% at midnight in January and May. Newly hatched *Themisto abyssorum* contributed substantially to mesozooplankton biomass at midnight in May, thus reducing the relative importance of *Calanus* spp. Patterns in the 0-100 m layer were very similar to the ones described for the 0-50 m layer, except for an even higher discrepancy between day and night biomass in September (Fig. 6). The large copepods dominated the mesozooplankton biomass in roughly the same proportions as for the 0-50 m layer in the same months. The contribution of chaetognaths to mesozooplankton biomass never exceeded 5% in the two layers over the different

426 months. In summary, evidence for strong DVM was essentially found in late September and the
427 behavior was most pronounced for the macrozooplankton, particularly *Thysanoessa* spp.
428
429 ***Diel migrant biomass from acoustic data***
430 In the 0-40 m layer, the monthly mean of euphausiid biomass was always higher at night than at
431 day from January to April, and from August to September (Fig. 7a). Euphausiid biomass showed
432 a first peak in February, with 0.9 g C m^{-2} at night, and a second peak of lesser magnitude in May-
433 June during the midnight sun and peak season of primary production. The range of euphausiid
434 biomass in January, estimated from the MIK net sampling a few days before the onset of
435 synchronous DVM (0.09-0.6 g m^{-2}), is comparable with the range derived from the AZFP data
436 for the entire study period (0.09-0.9 g m^{-2}). Likewise, night biomass estimates from the MIK nets
437 close to the September equinox (0.5-0.8 g m^{-2}) were within the same range, whereas the estimates
438 during the day were much lower (0.0008-0.001 g m^{-2}). The euphausiid migrant biomass, based on
439 day-night change, peaked in February-March (>0.6 g C m^{-2}) and reached a minimum in April
440 (0.09 g C m^{-2}) close to the onset of midnight sun (Fig. 7b). The pattern in the 2-82 m layer was
441 somewhat different from the observations in 2-40 m (Fig. 7c). First, the mean biomass was higher
442 during day than at night in January, a bias likely due to DVM occurring essentially over the top
443 40 m layer until late January. The second peak of euphausiid biomass (3.2 g C m^{-2}) in the midst
444 of midnight sun in June was higher then the first winter peak in March. Migrant biomass peaked
445 in February-March, remaining above 1 g C m^{-2}.
446
447 Classical DVM was also observed for copepods and chaetognaths prior to the onset of midnight
448 sun and in August-September in the 2-40 m layer (Fig. 8a and 9a). However, in the darkest
449 months of January and February, copepod biomass tended to be higher at day than at night (Fig.

8a) and difference between night and day values was much less marked for the copepod group than for euphausiids and chaetognaths. On the other hand, the latter two displayed similar patterns, although the biomass estimates for the chaetognaths were much less.

Copepod and chaetognath biomass increased in the surface layer in June, coinciding with the season of high primary production. Copepod biomass from AZFP data (0.2-0.3 g m^{-2}) fell within the range of biomass values estimated from mesozooplankton net sampling of the top 0-50 m layer in January and September (0.02-0.2 g m^{-2}). For copepods, a classic migrant biomass (shallower distribution at night and deeper at day) was first measured in March with a maximum of 0.03 g m^{-2} (Fig 8b). The migrant biomass of chaetognaths showed a pattern similar to the one for euphausiids in the top 40 and 82 m of the water column (Fig.9b and d).

Averaged over the entire study period, the migrant biomass of euphausiids was about 34 and 6 times higher than the sum of copepod and chaetognath biomass in the top 40 and 82 m layers, respectively.

Respiration and excretion per unit mass

Hourly rates of respiratory carbon loss per unit mass of the euphausiids *Thysanoessa* spp. in the uppermost 30 m varied little between January, May and September (range 0.48-0.51 µg C mg C^{-1} h^{-1}) (Table 2). The specific respiration of *Thysanoessa* spp. was in the same range as that of the other macrozooplankton taxa: *Themisto abyssorum* and *T. libellula*. Surprisingly, specific respiration of the two mesozooplankton size classes was high (>2.5 µg C mg C^{-1} h^{-1}) in January when food is supposed to be scarce. The respiration rate of the >1000 µm fraction in January was significantly higher than in May and September (Kruskal-Wallis test; $p = 0.0157$). For the 200-

1000-µm fraction, the respiration was only significantly higher in January than in September (Kruskal-Wallis test; $p = 0.0007$).

The euphausiid *Thysanoessa* spp. showed higher specific hourly rates of ammonium excretion around the September equinox (0.06 ± 0.03 µg N mg C^{-1} h^{-1}) than during the polar night (0.03 ± 0.01 µg N mg C^{-1} h^{-1}) (Kruskal-Wallis test; $p = 0.0058$). The specific excretion rate of the large and small mesozooplankton, however, did not differ between January and September, contrary to what was observed in the case of respiration. Pooling together the values of January and September yielded mean specific excretion rates of 0.97 ± 0.89 and 0.62 ± 0.27 µg N mg C^{-1} h^{-1} for the large and small mesozooplankton, respectively.

Community metabolism and active C and N transport

For euphausiids, the mean of all measured specific respiration (0.50 ± 0.20 µg C mg C^{-1} h^{-1}) was used to calculate the community respiration in the top layers and the active respiratory transport of carbon (equation 5) below the targeted depths. For excretion rates, it was assumed that the low rate measured for euphausiids in January (0.03 ± 0.01 µg N mg C^{-1} h^{-1}) persisted until April, before the onset of primary production. The higher rate (0.06 ± 0.03 µg N mg C^{-1} h^{-1}) was then applied for the remaining of the study period to estimate community ammonium excretion and active transport of nitrogen. The reasons for the higher specific respiration rate of mesozooplankton in January compared to May and September are unknown, but most likely not due to strong feeding activity. This complicated the selection of logical cut-off points between January and May to discriminate periods when different specific respiration rates should be applied. Therefore, the specific respiration rates for January, May and September were pooled to give a mean specific respiration rate of mesozooplankton of 1.75 ± 1.06 µg C mg C^{-1} h^{-1} that was

498 used to calculate community daily respiration and active carbon flux due to DVM. Since there
499 was no difference in ammonium excretion rate per unit mass measured in January and September,
500 the mean specific excretion rates of 0.97 ± 0.89 μg N mg C^{-1} h^{-1} was applied in the equations.
501
502 Because of the high variability in the euphausiid biomass in the top layers, the monthly
503 respiratory carbon loss of the euphausiid community was variable (Table 3). In the uppermost 40
504 m, community respiration remained above 4 mg C m^{-2} d^{-1} from January to March, at the height of
505 winter DVM activity (Fig. 7). Daily respiration dropped in April when zooplankton spent only a
506 few hours a day in the surface layer (Fig. 4), before recovering during the midnight sun period in
507 May-June at the onset of the spring bloom period (Fig. 3). In the post-bloom conditions of July to
508 early September, respiration reached again low levels compared to the winter and bloom periods.
509 In the uppermost 82 m of the water column, euphausiid respiration showed a pattern similar to
510 the one for the 0-40 m layer in winter and late summer. However, maximum respiration (>38 mg
511 C m^{-2} d^{-1}) was reached in June when fluorescence at 37 m depth peaked.
512
513 Copepods showed less variability and seasonal fluctuation in their daily respiration than did
514 euphausiids (Table 3). Throughout the study period, the community respiration ranged from 8-14
515 and 10-43 mg C m^{-2} d^{-1} in the 2-40 m and 2-82 m layers, , respectively, with the highest values in
516 June. Overall, copepod community respiration was approximately 2 times higher than euphausiid
517 respiration in the top 40 m while they were the same in the top 80 m of the water column.
518 Chaetognath respiration was lower, being 43 and 19 times less than copepod and euphausiid
519 respiration, respectively, in the top 40 m. The daily active respiratory transport of carbon due to
520 copepod and chaetognath DVM peaked in March-April . Averaged over the study period,

521 euphausiids exported 10 and 3 times more carbon during their DVM out of the top 40 and 82 m
522 layers respectively than copepods, and about 18 times more than chaetognaths for the two layers.
523
524 The highest estimates of euphausiid community excretion of ammonium were found during the
525 main primary production season in May-June in the uppermost 40 m (>0.7 mg N m^{-2} d^{-1}) and
526 June-July in the 2-82 layer (>2 mg N m^{-2} d^{-1}) (Table 4). During the winter months and the post-
527 bloom period, the stable daily excretion ranged 0.1-0.5 and 0.4-1.9 mg N m^{-2} d^{-1} in the two top
528 layers. The DVM-mediated export of nitrogen out of the 40 and 82 m top layers was lower at the
529 end and right after the polar night (January-February), and at the start of the midnight sun prior to
530 the spring bloom (April).
531
532 Copepod daily excretion of ammonium was about 14 and 6 times the euphausiid excretion in the
533 2-40 and 2-82 m surface layers, respectively. Copepod excretion reached a maximum in June
534 with a steep peak in the 2-82 m layer (24 mg N m^{-2} d^{-1}). Active export of N due to copepod DVM
535 culminated in March-April. On average, copepods transported 30% more N out of uppermost 40
536 m than euphausiids and 4 times more from the 2-82 m layer during the winter period. On the
537 other hand, euphausiids exported 30% more and 6% less N than copepods did from the same two
538 layers, respectively, during the post-bloom period. In comparison with euphausiids and copepods,
539 chaetognaths had lower excretion rates that were never >0.8 mg N m^{-2} d^{-1} in the two studied
540 layers. Their capacity to transport N below these layers was thus low compared to the two other
541 zooplankton groups.
542
543 **Sinking flux of POC and PON**

544 Sinking POC flux integrated over the winter period 21 January-3 April was 0.7 g m^{-2} at 40 m
545 depth in 2014, and 2.1 g m^{-2} at 100 m depth in 2013. Over the period 9 August-6 September,
546 similar in duration to the autumn DVM period sampled in our study (11 August-9 September),
547 the POC flux was 0.7 g m^{-2} at 100 m depth in 2013.
548
549 In the same winter period as above, the sinking PON flux was 0.25 g m^{-2} at 40 m depth in 2014,
550 and 0.37 g m^{-2} at 100 m depth in 2013. In the autumn period, the PON flux was 0.12 g m^{-2} at 100
551 m depth in 2013.
552
553 **Discussion**
554 ***Seasonal variability in diel vertical migration***
555 The visual analysis of the data from the moored AZFP multifrequency echosounder identified
556 classical DVM from the end of January to mid-April, and recorded the onset of autumn DVM in
557 mid-August (Fig. 3). Previous observations at the same site based on ADCP data collected from
558 2006 to 2008 suggest that the autumn DVM period lasted until mid-November (Wallace et al.
559 2010), which would make the two DVM phases equal in duration. During the DVM periods,
560 zooplankton moved synchronously in and out of the uppermost layer of the water column over
561 depth ranges of 40 m (depth of sediment traps) and 82 m (deepest threshold sampled by the
562 AZFP) that are relevant for vertical fluxes of elements. Covering almost the entire water column,
563 the ADCP echogram in late September showed DVM amplitudes of 120-140 m at the autumn
564 equinox (Fig. 4). The two periods of classical synchronous DVM were out of phase with the
565 period of high pelagic primary productivity, most probably reducing the contribution of active
566 transport to the biological pump. Such uncoupling between DVM and the phytoplankton bloom
567 was also observed in 2007 and 2008 in Kongsfjorden (Wallace et al. 2010), and this pattern is

568 likely the rule rather than the exception in high-Arctic ecosystems. Here, there is generally a
569 single bloom, usually between late April and August (Daase et al. 2013), and during a period of
570 reduced diel light variation due to midnight sun. With the ongoing loss of Arctic sea ice, many
571 regions at the periphery of the shrinking perennial ice pack are developing a second bloom in the
572 autumn (Ardyna et al. 2014), and it is likely that this will coincide with the autumn DVM phase.
573 Thus, we can expect classic DVM to have a growing role in the biological pump if these
574 observed changes in phytoplankton seasonality amplify in the future.
575
576 Combining the AZFP data analysis with morphometric information on zooplankton caught in
577 nets allowed us to identify euphausiids as the major diel migrants in terms of biomass in the fjord
578 in 2014. This finding was further validated with plankton net data limited to January and
579 September that showed that euphausiids of the genus *Thysanoessa* made up the bulk of
580 macrozooplankton biomass (>90%) at night. We also attributed the high backscatter in the
581 surface layer in June to the presence of *Thysanoessa* spp., although macrozooplankton were not
582 sampled quantitatively with nets during the spring-summer season due to the unavailability of a
583 ship large enough for trawling large plankton nets. Temperature profiles above 2^{o}C throughout
584 the water column in May and July revealed no significant intrusion of cold Arctic Water into
585 Kongsfjorden. Furthermore, mesozooplankton data from the same period indicate no change in
586 the community that could have signalled a massive advection of Arctic zooplankton. Thus, we
587 assumed that the macrozooplankton size class, dominated by the arcto-boreal *Thysanoessa* spp.
588 during winter, did not shift either to a more Arctic assemblage during the period of high
589 biological production. It is possible, however, that larger macrozooplankton like the more
590 Atlantic *Meganyctiphanes norvegica* were underestimated in the net samples as they could
591 possibly avoid the net type and trawl short duration used.

592

593 Large copepods (dominated by *Calanus* spp.) and chaetognaths (essentially *Parasagitta elegans*)
594 also performed diel migrations during the two DVM periods. Nevertheless, zooplankton biomass
595 derived from the calibrated AZFP revealed that euphausiids generally contributed >90% of the
596 total diel migrant biomass (euphausiids + copepods + chaetognaths) in the uppermost 40 m and
597 82 m. The unverified assumption of a monospecific zooplankton assemblage in each echo-
598 integration cell of the acoustic analysis may have had an effect on the estimation of biomass that
599 is difficult to evaluate. However, we are confident that the small size selected for the cells (1-
600 meter vertical by 5-minutes horizontal) tempers this effect. The daily zooplankton migrant
601 biomass below 82 m during the transition from polar night to midnight sun and in late summer in
602 Kongsfjorden exceeded most of the estimates for other where active fluxes due to DVM were
603 studied (Table S3). Our range of estimates did encompass the higher values measured off the
604 Canary Islands and in the North Pacific (Steinberg et al. 2008; Takahashi et al. 2009; Yebra et al.
605 2005). One of the plausible reasons for the discrepancy between our high estimates and those of
606 other studies is that most of these others did not include the macrozooplankton size class, which
607 dominated zooplankton migrant biomass in Kongsfjorden. Therefore, their assessment of the
608 importance of zooplankton active fluxes of carbon and nitrogen may well be very conservative.
609

610 ***Zooplankton metabolism***

611 This study significantly expands on the limited knowledge of respiration and ammonium
612 excretion rates of arctic euphausiids. The mass-specific respiration rates of *Thysanoessa* spp.
613 (mainly *T. inermis*) in winter, spring and autumn 2014 were close to the value found in April
614 (pre-bloom period) and August (post-bloom) for *T. inermis* in Kongsfjorden (Huenerlage et al.
615 2015), and within the range of values in late May in the eastern Barents Sea (Ikeda and Skjoldal

616 1989). We did not observe a lower specific respiration during the polar night period of food
617 scarcity compared to the pre-bloom period or to the autumn equinox, supporting the suggestion of
618 Huenerlage et al. (2015) that *Thysanoessa* spp. do not reduce their metabolism in winter. It is
619 possible that respiration rates were higher during the bloom period, between late May and June,
620 when the mainly herbivore *Thysanoessa inermis* ingests large quantities of pelagic algae to build
621 its lipid reserves. If so, our estimates of euphausiid community respiration for the summer period
622 would be conservative. Mass-specific ammonium-excretion rates of *Thysanoessa* spp. in our
623 study are consistent with those measured by Ikeda and Skjoldal (1989) and Huenerlage et al.
624 (2015). The lower excretion rate in January than in September is presumably due to better
625 feeding conditions in autumn, as excretion and ingestion rates are closely linked (Saborowski et
626 al. 2002).
627
628 Overall, mesozooplankton respiration rates reported here are consistent with measurements on
629 the same size classes during the Antarctic summer (Hernández-León et al. 1999), and the highest
630 value measured on total mesozooplankton (not size-fractionated) from north-Svalbard in summer
631 (Alcaraz et al. 2010). But we measured higher mass-specific respiration rates than Welch et al.
632 (1997) did in the colder waters of the Canadian Arctic archipelago. Likewise, mesozooplankton
633 ammonium excretion rates in Kongsfjorden were 1-3.5 times higher than the rates for Antarctica
634 and north-Svalbard (Table 2).
635
636 Pelagic primary production estimates in Kongsfjorden are scarce and not available for 2014.
637 Hodal et al. (2012) calculated a gross primary production (GPP) of 27–35 g C m^{-2} in the 0-40 m
638 layer during the spring bloom of 2002 (18 April-13 May), consistent with previous annual GPP
639 estimates of 25-30 g C m^{-2} in the northeast Barents Sea (Hegseth 1998). Thus, assuming the same

range of GPP in 2014 as in 2002, euphausiids would have used 0.7-0.9% and large copepods 1.3-1.7% of the phytoplankton carbon produced to cover their respiratory carbon loss (Rc) during the bloom, here circumscribed to 15 May-20 June. These fractions are much less than the 5-67% (average 23%) of GPP that mesozooplankton respiration alone accounted for in the northwest Barents Sea (Alcaraz et al. 2010). However, it is important to bear in mind that our metabolic measurements were not made during bloom conditions and, thus, are likely underestimates of respiration and excretion during the bloom period. A rough estimate of zooplankton ingestion (I), using the equation of Ikeda and Motoda (1978) in which I= 2.5Rc, shows that combined euphausiid-copepod grazing would account for 5-6% of GPP, a range below the 22-44% of GPP intercepted by zooplankton in the northeast Barents Sea (Wexels Riser et al. 2008), or 45% by copepods in the Greenland Northeast Water Polynya (Daly 1997). Using the Redfield ratio to convert phytoplankton carbon production to nitrogen production, euphausiid and mesozooplankton $NH4^+$ excretion in the uppermost 40 m would support 5-7% of the bloom GPP. This is again low compared to the 9-242% (mean 59%) that mesozooplankton alone re-supplied in the photic layer of the northern Barents Sea for phytoplankton production in July (Alcaraz et al. 2010). Therefore, we suggest that the effect of zooplankton grazing and excretion on phytoplankton total production was weak in Kongsfjorden during the bloom of 2014.

Active export of dissolved carbon and nitrogen mediated by DVM

The active transport of carbon due to synchronous migration by euphausiids, large copepods and chaetognaths was 0.3 and 0.9 g m^{-2} below 40 m and 82 m depth, respectively, during the 2014 winter DVM period in Kongsfjorden (31 January-11 April), and 0.2 g m^{-2} below 82 m at the onset of the autumn DVM (from 11 August to 9 September). Thus, the DVM-mediated carbon transport would represent >40% of the winter carbon sinking flux of POC measured in sediment

664 traps, and >25% of the sinking flux during the first weeks of autumn. These ratios of active to
665 passive carbon export fall within the range of ratios for daily fluxes (13-70%) in several
666 oligotrophic and more seasonally stable sub-Arctic to equatorial systems (Dam et al. 1995;
667 Hernández-León et al. 2001; Stukel et al. 2013; Yebra et al. 2005; Zhang and Dam 1997) (Table
668 S3). Representing >25% of POC sinking flux, the DVM transport in Kongsfjorden was higher
669 than other estimates (1-14% of sinking flux) for different times of the year in the subtropical
670 Atlantic, Bermuda, around the Canary Islands, and from equatorial to subarctic Pacific regions
671 (Kobari et al. 2008; Le Borgne and Rodier 1997; Putzeys et al. 2011; Rodier and Le Borgne
672 1997). The 0.9 g C m^{-2} transported by winter DVM in Kongsfjorden represents 30% of the active
673 flux by *Calanus* spp. (mainly *C. hyperboreus*) seasonal vertical migration (SVM) below 100 m
674 (3.1 g C m^{-2}) during the overwintering period (October-April) in the southeastern Beaufort Sea
675 (Darnis and Fortier 2012). Adding the amount transported to depth by autumn DVM could
676 possibly double the contribution of DVM-mediated transport over an annual cycle. Using short-
677 term sediment trap deployments (21-52 h) in Kongsfjorden in 2012-2013, Lalande et al. (2016)
678 provide three estimates of daily sinking POC fluxes: during a bloom in May, and post-bloom
679 conditions in August and October (Table S5). Comparison between daily active transport below
680 82 m and the mean post-bloom POC flux in 2012 (167 ± 88 mg C m^{-2} d^{-1} at 100 m) yields active
681 to passive export ratios from 4-12% that are within the range of low ratios published. To estimate
682 the active transports, the zooplankton groups were assumed not to feed at depth. This may have
683 been the case for copepods and euphausiids but not for the carnivorous chaetognaths. However,
684 the latter represented a minor fraction of the migrant biomass. Although not ideal, such
685 comparisons involving different years, locations, and seasons reveal all the same that, despite the
686 complex DVM regime at high latitudes, the active carbon transport due to DVM in Kongsfjorden
687 is close to what has been reported in lower latitude regions of the World Ocean.

688

689 Zooplankton winter DVM transported 0.03 and 0.18 g N m^{-2} out of the 40 and 82 m top water
690 layers, respectively, whereas early autumn DVM transported 0.04 g N m^{-2} out the 100 m top
691 layer. The DVM-mediated active transport of nitrogen represents thus 12 and 49% of the PON
692 sinking flux at 40 and 100 m integrated over the winter period, and 33% of the sinking flux at
693 100 m in early autumn. Such ratios of active to passive export of nitrogen fall well within the
694 wide range of ratios (7-108% of daily PON flux) stemming from the few studies addressing
695 active transport of nitrogen due to DVM (Al-Mutairi and Landry 2001; Longhurst et al. 1989;
696 Longhurst and Harrison 1988; Steinberg et al. 2002) (Table S4). On a daily basis, however,
697 estimates of active N transport due to euphausiid, copepod and chaetognath represent 4-18% of
698 the mean sinking flux of PON (21 ± 7 mg N m^{-2} d^{-1}) below 100 m during the post-bloom
699 conditions in 2012 (Table S5). Our daily ratios thus lie at the lower range of published ratios.
700 Interestingly, winter DVM and excretion at depth by large copepods contributed 76% of the
701 active N transport, whereas it was euphausiid DVM and their respiration at depth that dominated
702 in similar proportion (70%) the active C transport during the same period.
703

704 By using acoustic data with measurements of respiration and ammonium excretion, we have been
705 able to describe for the first time the role of zooplankton DVM in the functioning of the
706 biological pump of a high-latitude marine ecosystem. As expected, the active transport of carbon
707 and nitrogen to depth through synchronous DVM is discontinuous over an annual cycle, due to
708 the suspension of DVM during parts of the polar night and midnight sun (Berge et al. 2009;
709 Cottier et al. 2006; Last et al. 2016). The fact that this process occurs essentially outside of the
710 short season of high photosynthesis likely limits its function in the biological pump of Arctic
711 ecosystems if an annual budget is to be estimated. On the other hand, this study also revealed that

712 the importance of active transport in the Kongsfjorden ecosystem during times of strong DVM
713 (winter and autumn) compared well with other oceanic systems. Since the winter DVM took
714 place in a fully mixed water column in Kongsfjorden, the active transports estimated for winter
715 cannot be regarded as export fluxes. But at other times of the year (Loeng 1991) and in other
716 locations in the Arctic, DVM coincides with highly stratified water columns. Production of
717 sinking fecal pellets, active transport of feces in the migrants' guts, high winter mortality at
718 depth, and shedding of exuviae, should also be quantified and included in C and N budgets along
719 with DVM-mediated flux of dissolved components measured here. If we are to achieve a realistic
720 description of the biological pump of the Arctic marine ecosystems it will be especially important
721 to estimate these rates during the understudied periods outside of the short spring-summer season.
722 Based on our results, it remains that respiratory C and excretory N transport due to DVM should
723 be considered for flux estimation in the extensive Arctic regions permanently subject to haline
724 stratification. Under the effect of global warming, the increased river runoff and sea ice melt will
725 result in a better match in timing between DVM-mediated processes and stratification of the
726 water column (Pemberton and Nilsson 2016), which should increase the efficiency of the
727 biological carbon pump. Furthermore, Cottier et al. (2006) and Wallace et al. (2010) found
728 evidence for unsynchronized migration in Kongsfjorden during the midnight sun in June.
729 Zooplankton would swim individually in the surface layer, possibly to feed, and sink out during
730 digestion repeatedly over a 24-h period. In 2014, June coincided with maximum fluorescence and
731 zooplankton biomass in the 82 m surface layer. Direct vertical shunting of carbon and nitrogen to
732 deeper less retentive layers due to this foray-type migration would enhance the efficiency of the
733 biological pump when biological productivity is at its highest. However, unsynchronized
734 migration needs to be investigated in other high-latitude regions. For instance, no unsynchronized

735 migrations were detected during the midnight sun in the Antarctic Weddell Sea (Cisewski and
736 Strass 2016) and over the West Spitsbergen outer shelf (Geoffroy et al. 2016).
737
738 The finding of the prominent role of euphausiids (particularly *Thysanoessa* spp.) in the active
739 vertical transport of carbon has also been reported lately in the North-west Mediterranean Sea
740 (Isla et al. 2015). Euphausiids are abundant in the shelf seas on the Pacific side of the Arctic as
741 well (Eisner et al. 2013) where there is a stronger stratification of the water column. Over the
742 Arctic continental slopes and basins, little is known about the distribution of macrozooplankton
743 and it is assumed so far that long-range SVM by large *Calanus hyperboreus* is the main pathway
744 for the active vertical flux of carbon (Darnis and Fortier 2012; Hirche 1997). To be able to fully
745 assess the function of zooplankton migrations in the biological pump on a pan-Arctic scale, we
746 need to define better the biogeography, feeding biology and migratory parameters (depth range,
747 swimming speed, time at depth) of key zooplankton taxa, namely the Arctic *Calanus* spp., the
748 arcto-boreal *Thysanoessa* spp. and other macrozooplankton like *Themisto* spp.
749
750 **References**
751 A.S.L. 2014. AZFP (Acoustic Zooplankton Fish Profiler) Operators Manual. , p. 77. ASL.
752 Al-Mutairi, H., and M. R. Landry. 2001. Active export of carbon and nitrogen at Station ALOHA
753 by diel migrant zooplankton. Deep Sea Res., Part II **48:** 2083-2103.
754 Alcaraz, M. and others 2010. The role of arctic zooplankton in biogeochemical cycles: respiration
755 and excretion of ammonia and phosphate during summer. Polar Biol. **33:** 1719-1731.
756 Ardyna, M., M. Babin, M. Gosselin, E. Devred, L. Rainville, and J.-É. Tremblay. 2014. Recent
757 Arctic Ocean sea ice loss triggers novel fall phytoplankton blooms. Geophys. Res. Lett.**:**
758 2014GL061047.

759 Basedow, S. L., K. Eiane, V. Tverberg, and M. Spindler. 2004. Advection of zooplankton in an
760 Arctic fjord (Kongsfjorden, Svalbard). Estuar. Coast. Shelf Sci. **60:** 113-124.
761 Benfield, M. C., C. S. Davis, and S. M. Gallager. 2000. Estimating the in-situ orientation of
762 *Calanus finmarchicus* on Georges Bank using the Video Plankton Recorder. Plankton
763 Biology & Ecology **47:** 69-72.
764 Berge, J. and others 2009. Diel vertical migration of Arctic zooplankton during the polar night.
765 Biol. Lett. **5:** 69-72.
766 Berge, J. and others 2014. Arctic complexity: a case study on diel vertical migration of
767 zooplankton. J. Plankton Res. **36:** 1279-1297.
768 Berge, J. and others 2015. In the dark: A review of ecosystem processes during the Arctic polar
769 night. Progr. Oceanogr. **139:** 258-271.
770 Brierley, A. S. 2014. Diel vertical migration. Curr. Biol. **24:** R1074-R1076.
771 Bronk, D. A., and D. K. Steinberg. 2008. Chapter 8 - Nitrogen Regeneration, p. 385-467. *In* D. G.
772 Capone, D. A. Bronk, M. R. Mulholland and E. J. Carpenter [eds.], Nitrogen in the
773 Marine Environment (2nd Edition). Academic Press.
774 Chu, D., K. G. Foote, and T. K. Stanton. 1993. Further analysis of target strength measurements
775 of Antarctic krill at 38 and 120 kHz: Comparison with deformed cylinder model and
776 inference of orientation distribution. The Journal of the Acoustical Society of America **93:**
777 2985-2988.
778 Cisewski, B., and V. H. Strass. 2016. Acoustic insights into the zooplankton dynamics of the
779 eastern Weddell Sea. Progr. Oceanogr. **144:** 62-92.
780 Cottier, F., V. Tverberg, M. Inall, H. Svendsen, F. Nilsen, and C. Griffiths. 2005. Water mass
781 modification in an Arctic fjord through cross-shelf exchange: The seasonal hydrography
782 of Kongsfjorden, Svalbard. J. Geophys. Res. **110**.

783 Cottier, F. R., F. Nilsen, M. E. Inall, S. Gerland, V. Tverberg, and H. Svendsen. 2007.
784 Wintertime warming of an Arctic shelf in response to large-scale atmospheric circulation.
785 Geophys. Res. Lett. **34**.
786 Cottier, F. R., F. Nilsen, R. Skogseth, V. Tverberg, J. Skarðhamar, and H. Svendsen. 2010. Arctic
787 fjords: a review of the oceanographic environment and dominant physical processes.
788 Geological Society, London, Special Publications **344:** 35-50.
789 Cottier, F. R., G. A. Tarling, A. Wold, and S. Falk-Petersen. 2006. Unsynchronized and
790 synchronized vertical migration of zooplankton in a high arctic fjord. Limnol. Oceanogr.
791 **51:** 2586-2599.
792 Daase, M., K. Eiane, D. L. Aksnes, and D. Vogedes. 2008. Vertical distribution of *Calanus* spp.
793 and *Metridia longa* at four Arctic locations. Mar. Biol. Res. **4:** 193-207.
794 Daase, M. and others 2013. Timing of reproductive events in the marine copepod *Calanus*
795 *glacialis*: a pan-Arctic perspective. Can. J. Fish. Aquat. Sci. **70:** 871–884.
796 Daly, K. L. 1997. Flux of particulate matter through copepods in the Northeast Water Polynya. J.
797 Mar. Syst. **10:** 319-342.
798 Dam, H. G., M. R. Roman, and M. J. Youngbluth. 1995. Downward export of respiratory carbon
799 and dissolved inorganic nitrogen by diel-migrant mesozooplankton at the JGOFS
800 Bermuda time-series station. Deep Sea Res., Part I **42:** 1187-1197.
801 Darnis, G., and L. Fortier. 2012. Zooplankton respiration and the export of carbon at depth in the
802 Amundsen Gulf (Arctic Ocean). Journal of Geophysical Research **117:** C04013.
803 Ducklow, H. W., D. K. Steinberg, and K. O. Buesseler. 2001. Upper Ocean Carbon Export and
804 the Biological Pump. Oceanography **14:** 50-58.

Eisner, L., N. Hillgruber, E. Martinson, and J. Maselko. 2013. Pelagic fish and zooplankton species assemblages in relation to water mass characteristics in the northern Bering and southeast Chukchi seas. Polar Biol. **36:** 87-113.

Fischer, J., and M. Visbeck. 1993. Seasonal variation of the daily zooplankton migration in the Greenland Sea. Deep-Sea Res. Part I-Oceanogr. Res. Pap. **40:** 1547-1557.

Fortier, M., L. Fortier, H. Hattori, H. Saito, and L. Legendre. 2001. Visual predators and the diel vertical migration of copepods under Arctic sea ice during the midnight sun. J. Plankton Res. **23:** 1263-1278.

Geoffroy, M., F. R. Cottier, J. Berge, and M. E. Inall. 2016. AUV-based acoustic observations of the distribution and patchiness of pelagic scattering layers during midnight sun. ICES J. Mar. Sci. DOI:10.1093/icesjms/fsw158.

Gnaiger, E. 1983. Calculation of energetic and biochemical equivalents of respiratory oxygen consumption, p. 337-345. *In* E. Gnaiger and H. Forstner [eds.], Polarographic oxygen sensors : aquatic and physiological applications. Springer-Verlag.

Hegseth, E. N. 1998. Primary production of the northern Barents Sea. Polar Res. **17:** 113-123.

Hegseth, E. N., and V. Tverberg. 2013. Effect of Atlantic water inflow on timing of the phytoplankton spring bloom in a high Arctic fjord (Kongsfjorden, Svalbard). J. Mar. Syst. **113:** 94-105.

Hernández-León, S., M. Gomez, M. Pagazaurtundua, A. Portillo-Hahnefeld, I. Montero, and C. Almeida. 2001. Vertical distribution of zooplankton in Canary Island waters: implications for export flux. Deep Sea Res., Part I **48:** 1071-1092.

Hernández-León, S., S. Torres, M. Gomez, I. Montero, and C. Almeida. 1999. Biomass and metabolism of zooplankton in the Bransfield Strait (Antarctic Peninsula) during austral spring. Polar Biol. **21:** 214-219.

829 Hirche, H.-J. 1997. Life cycle of the copepod *Calanus hyperboreus* in the Greenland Sea. Mar.
830 Biol. **128:** 607-618.
831 Hodal, H., S. Falk-Petersen, H. Hop, S. Kristiansen, and M. Reigstad. 2012. Spring bloom
832 dynamics in Kongsfjorden, Svalbard: nutrients, phytoplankton, protozoans and primary
833 production. Polar Biol. **35:** 191-203.
834 Huenerlage, K., M. Graeve, C. Buchholz, and F. Buchholz. 2015. The other krill: overwintering
835 physiology of adult *Thysanoessa inermis* (Euphausiacea) from the high-Arctic
836 Kongsfjord. Aquat. Biol. **23:** 225-235.
837 Ikeda, T., and S. Motoda. 1978. Estimated Zooplankton Production and Their Ammonia
838 Excretion in Kuroshio and Adjacent Seas. Fishery Bulletin **76:** 357-367.
839 Ikeda, T., and H. R. Skjoldal. 1989. Metabolism and elemental composition of zooplankton from
840 the Barents Sea during early Arctic summer. Mar. Biol. **100:** 173-183.
841 Ingvarsdóttir, A., D. F. Houlihan, M. R. Heath, and S. J. Hay. 1999. Seasonal changes in
842 respiration rates of copepodite stage V *Calanus finmarchicus* (Gunnerus). Fish. Oceanogr.
843 **8:** 73-83.
844 Isla, A., R. Scharek, and M. Latasa. 2015. Zooplankton diel vertical migration and contribution to
845 deep active carbon flux in the NW Mediterranean. J. Mar. Syst. **143:** 86-97.
846 Kobari, T., D. K. Steinberg, A. Ueda, A. Tsuda, M. W. Silver, and M. Kitamura. 2008. Impacts
847 of ontogenetically migrating copepods on downward carbon flux in the western subarctic
848 Pacific Ocean. Deep-Sea Res. Part II-Top. Stud. Oceanogr. **55:** 1648-1660.
849 Kristensen, Å., and J. Dalen. 1986. Acoustic estimation of size distribution and abundance of
850 zooplankton. Journal of Acoustical Society of America **80:** 601-611.
851 Kwasniewski, S., H. Hop, S. Falk-Petersen, and G. Pedersen. 2003. Distribution of Calanus
852 species in Kongsfjorden, a glacial fjord in Svalbard. J. Plankton Res. **25:** 1-20.

853 Lalande, C., B. Moriceau, A. Leynaert, and N. Morata. 2016. Spatial and temporal variability in
854 export fluxes of biogenic matter in Kongsfjorden. Polar Biol.**:** 1-14.
855 Last, Kim s., L. Hobbs, J. Berge, Andrew s. Brierley, and F. Cottier. 2016. Moonlight Drives
856 Ocean-Scale Mass Vertical Migration of Zooplankton during the Arctic Winter. Curr.
857 Biol. **26:** 1-8.
858 Lawson, G. L., P. H. Wiebe, C. J. Ashjian, S. M. Gallager, C. S. Davis, and J. D. Warren. 2004.
859 Acoustically-inferred zooplankton distribution in relation to hydrography west of the
860 Antarctic Peninsula. Deep Sea Res., Part II **51:** 2041-2072.
861 Le Borgne, R., and M. Rodier. 1997. Net zooplankton and the biological pump: a comparison
862 between the oligotrophic and mesotrophic equatorial Pacific. Deep Sea Res., Part II **44:**
863 2003-2023.
864 Loeng, H. 1991. Features of the oceanographic conditions of the Barents Sea. Pp. 5-18. *In* E.
865 Sakshaug, C. C. E. Hopkins and N. A. Øritsland [eds.], Proceedings of the Pro Mare
866 Symposium on Polar Marine Ecology. Trondheim, 12-16 May 1990. Polar Research 10
867 (1).
868 Longhurst, A. R. and others 1989. NFLUX-A test of vertical nitrogenflux by diel migrant biota.
869 Deep Sea Res., Part A **36:** 1705-1719.
870 Longhurst, A. R., A. W. Bedo, W. G. Harrison, E. J. H. Head, and D. D. Sameoto. 1990. Vertical
871 flux of respiratory carbon by oceanic diel migrant biota. Deep Sea Res., Part I **37:** 685-
872 694.
873 Longhurst, A. R., and W. G. Harrison. 1988. Vertical nitrogen flux from the oceanic photic zone
874 by diel migrant zooplankton and nekton. Deep Sea Res., Part A **35:** 881-889.

875 Marinov, I., and J. L. Sarmiento. 2004. The role of the oceans in the global carbon cycle: an
876 overview, p. 395. *In* M. Follows and T. Oguz [eds.], The ocean carbon cycle and climate.
877 Kluwer Academic Publishers.
878 Parker-Stetter, S. L., L. G. Rudstam, P. J. Sullivan, and D. M. Warner. 2009. Standard operating
879 procedures for fisheries acoustic surveys in the Great Lakes. Great Lakes Fish. Comm.
880 Spec. Pub. 09-01.
881 Pemberton, P., and J. Nilsson. 2016. The response of the central Arctic Ocean stratification to
882 freshwater perturbations. Journal of Geophysical Research: Oceans **121:** 792-817.
883 Putzeys, S., L. Yebra, C. Almeida, P. Becognee, and S. Hernandez-Leon. 2011. Influence of the
884 late winter bloom on migrant zooplankton metabolism and its implications on export
885 fluxes. J. Mar. Syst. **88:** 553-562.
886 Ringelberg, J. 2010. Diel Vertical Migration of Zooplankton in Lakes and Oceans. Causal
887 Explanations and Adaptive Significances. Springer.
888 Rodier, M., and R. Le Borgne. 1997. Export flux of particles at the equator in the western and
889 central Pacific ocean. Deep-Sea Res. Part II-Top. Stud. Oceanogr. **44:** 2085-2113.
890 Saborowski, R., S. Brohl, G. A. Tarling, and F. Buchholz. 2002. Metabolic properties of Northern
891 krill, Meganyctiphanes norvegica, from different climatic zones. I. Respiration and
892 excretion. Mar. Biol. **140:** 547-556.
893 Seuthe, L., K. R. Iversen, and F. Narcy. 2011. Microbial processes in a high-latitude fjord
894 (Kongsfjorden, Svalbard): II. Ciliates and dinoflagellates. Polar Biol. **34:** 751-766.
895 Solórzano, L. 1969. Determination of ammonia in natural waters by the phenolhypochlorite
896 method. Limnol. Oceanogr. **14:** 799-801.

897 Stanton, T. K., and D. Chu. 2000. Review and recommendations for the modelling of acoustic
898 scattering by fluid-like elongated zooplankton: euphausiids and copepods. ICES Journal
899 of Marine Science: Journal du Conseil **57:** 793-807.
900 Stanton, T. K., D. Chu, and P. H. Wiebe. 1998. Sound scattering by several zooplankton groups.
901 II. Scattering models. The Journal of the Acoustical Society of America **103:** 236-253.
902 Stanton, T. K. and others 1994. On acoustic estimates of zooplankton biomass. ICES Journal of
903 Marine Science: Journal du Conseil **51:** 505-512.
904 Steinberg, D. K., C. A. Carlson, N. R. Bates, S. A. Goldthwait, L. P. Madin, and A. F. Michaels.
905 2000. Zooplankton vertical migration and the active transport of dissolved organic and
906 inorganic carbon in the Sargasso Sea. Deep Sea Res., Part I **47:** 137-158.
907 Steinberg, D. K., S. A. Goldthwait, and D. A. Hansell. 2002. Zooplankton vertical migration and
908 the active transport of dissolved organic and inorganic nitrogen in the Sargasso Sea.
909 Deep-Sea Res. Part I-Oceanogr. Res. Pap. **49:** 1445-1461.
910 Steinberg, D. K., B. a. S. Van Mooy, K. O. Buesseler, P. W. Boyd, T. Kobari, and D. M. Karl.
911 2008. Bacterial vs. zooplankton control of sinking particle flux in the ocean's twilight
912 zone. Limnol. Oceanogr. **53:** 1327-1338.
913 Stukel, M. R., M. D. Ohman, C. R. Benitez-Nelson, and M. R. Landry. 2013. Contributions of
914 mesozooplankton to vertical carbon export in a coastal upwelling system. Mar. Ecol.
915 Prog. Ser. **491:** 47-65.
916 Svendsen, H. and others 2002. The physical environment of Kongsfjorden-Krossfjorden, an
917 Arctic fjord system in Svalbard.
918 Takahashi, K., A. Kuwata, H. Sugisaki, K. Uchikawa, and H. Saito. 2009. Downward carbon
919 transport by diel vertical migration of the copepods Metridia pacifica and Metridia

okhotensis in the Oyashio region of the western subarctic Pacific Ocean. Deep Sea Res. Part I **56:** 1777-1791.

Wallace, M. I., F. R. Cottier, J. Berge, G. A. Tarling, C. Griffiths, and A. S. Brierley. 2010. Comparison of zooplankton vertical migration in an ice-free and a seasonally ice-covered Arctic fjord: An insight into the influence of sea ice cover on zooplankton behavior. Limnol. Oceanogr. **55:** 831-845.

Welch, H. E., T. D. Siferd, and P. Bruecker. 1996. Population densities, growth, and respiration of the chaetognath *Parasagitta elegans* in the Canadian high Arctic. Can. J. Fish. Aquat. Sci. **53:** 520-527.

---. 1997. Marine zooplanktonic and benthic community respiration rates at Resolute, Canadian high Arctic. Can. J. Fish. Aquat. Sci. **54:** 995-1005.

Wexels Riser, C., P. Wassmann, M. Reigstad, and L. Seuthe. 2008. Vertical flux regulation by zooplankton in the northern Barents Sea during Arctic spring. Deep Sea Res., Part II **55:** 2320-2329.

Willis, K., F. Cottier, S. Kwasniewski, A. Wold, and S. Falk-Petersen. 2006. The influence of advection on zooplankton community composition in an Arctic fjord (Kongsfjorden, Svalbard). J. Mar. Syst. **61:** 39-54.

Yebra, L., C. Almeida, and S. Hernandez-Leon. 2005. Vertical distribution of zooplankton and active flux across an anticyclonic eddy in the Canary Island waters. Deep Sea Res., Part I **52:** 69-83.

Zhang, X. S., and H. G. Dam. 1997. Downward export of carbon by diel migrant mesozooplankton in the central equatorial Pacific. Deep-Sea Res. Part II-Top. Stud. Oceanogr. **44:** 2191-2202.

Acknowledgments

We thank the crew of the R/V *Helmer-Hanssen* and *Teisten* as well as Kings Bay personnel in Ny-Ålesund and Daniel Vogedes for their precious assistance in logistics and sampling. This work would not have been possible without the help of Colin Griffiths, Estelle Dumont, Trine Callesen, Marit Reigstad, Marina Sanz-Martin, Catherine Lalande, Miriam Marquardt, Anna Vader, Carl Ballantine, Slawek Kwasniewski and the students of AB320/820 zooplankton course in 2014 (Morgan Bender, Heather Cronin, Ursula Ecker, Maeve McGovern, Sam Eglund Newby, Erik Haar Nielsen, Alejandro Prat, Pierre Priou, Mie Lundfryd Rasmussen, Petra Svaskova, Lotte Devries, Séan Mac Siúlaí, Sören Häfker, Helena Michelsen, Marc Silberberger). We wish to thank Hauke Flores and an anonymous reviewer for providing useful comments that helped improve this work substantially. The study is a contribution to: two NRC funded projects, Circa (NRC project number 214271) and Marine Night (NRC project number 226417), the Norwegian Polar Institute project N-ICE, and the Fjord and Coast Flagship of the FRAM-High North Research Centre for Climate and the Environment.

.

Figure legends

Fig. 1. Location of the sampling station KB3 in Kongsfjorden and of three moorings; one with an Acoustic Zooplankton Fish Profiler, one with two Acoustic Doppler Current Profilers, and another with fluorescence and PAR sensors (Table 1) The northward flowing West Spitsbergen Current (WSC; black arrow) and East Spitsbergen Current (ESC; dashed arrow) are illustrated.

967 Fig. 2. Vertical profiles of temperature, salinity and fluorescence at station KB3 in Kongsfjorden
968 at different dates of 2014.
969
970 Fig.3 (a) Time series of relative fluorescence (Norm. flsc.) at 37 m depth and backscatter for the
971 125 kHz frequency of the AZFP in Kongsfjorden from 17 January to 9 September 2014, and
972 expanded views of (a) winter DVM period (28-January-10 April) and (c) onset of autumn DVM
973 (10 August-9 September) defined qualitatively by visual analysis of the echogram.
974
975 Fig. 4. Backscatter from two 307.2 kHz ADCPs, one upward-looking and the other downward-
976 looking, from 23 to 25 September 2014 at the mooring site. Black and white vertical lines
977 indicate local midnights and middays as per the clock.
978
979 Fig. 5. Time series of time spent below 40 and 82 m depth by the high backscatter over a 24-h
980 cycle from January to September 2014. The horizontal broken line indicates the 12-h limit.
981
982 Fig. 6. Macro- and mesozooplankton biomass and composition from plankton net data in the
983 surface 30, 50 and 100-m layer at day and at night in January, May, July and September 2014 at
984 station KB3 in Kongsfjorden. “n” indicates number of plankton net deployments.
985
986 Fig. 7. Euphausiids. (a and c) time series of average monthly day and night biomass (± 1 SE) in
987 the 40 m and 82 m above the AZFP, respectively, and (b and d) respective diel migrant biomass
988 (± 1 SE) in the same layers, with *negative value indicating biomass during day higher than
989 night. Note different scales on the y-axis among panels.
990

991 Fig. 8. Copepods. (a and c) time series of average monthly day and night biomass (± 1 SE) in the
992 40 m and 82 m above the AZFP, respectively, and (b and d) respective diel migrant biomass (± 1
993 SE) in the same layers, with *negative value indicating biomass during day higher than night.
994 Note different scales on the y-axis among panels.
995
996 Fig. 9. Chaetognaths. (a and c) time series of average monthly day and night biomass (± 1 SE) in
997 the 40 m and 82 m above the AZFP, respectively, and (b and d) respective diel migrant biomass
998 (± 1 SE) in the same layers, with *negative value indicating biomass during day higher than
999 night. Note different scales on the y-axis among panels.
1000
1001 Supplemental Fig. S1. Example of a 125-kHz echogram with backscatters from fish schools and
1002 zooplankton.
1003
1004 Supplemental Fig. S2. Echograms at 125, 200 and 455 kHz of the AZFP in Kongsfjorden from
1005 17 January to 9 September 2014.
1006

1007 Table 1. Positions, periods of deployment and details on the moored instruments in Kongsfjorden

1008 used in the present study.

1009

1010

1011

Mooring	Bottom depth (m)	Latitude	Longitude	Deployed	Recovered	Instrumentation
AZFP 1	203	78°57.49'N	11°49.25'E	17 Jan 14	9 Sep 14	Upward AZFP 84 m Sediment trap 40 m
ADCP 1	231	78°57.76'N	11°47.93'E	23 Sep 14	25 Sep 14	Downward ADCP 96 m Upward ADCP 95 m Sediment trap 65 m
ADCP 2	236	78°57.75'N	11°48.30'E	05 Oct 13	09 Sep 14	ADCP 108 m ADCP 102 m Sediment trap 100 m Sediment trap 50 m Fluor. sensor 37 m PAR sensor 37 m
ADCP 3	243	78°57.73'N	11°48.43'E	01 Oct 12	06 Sep 13	ADCP 108 m ADCP 102 m Sediment trap 105 m Sediment trap 50 m Fluor. sensor 38 m PAR sensor 38 m

1012

1013

1014

1015

1016 Table 2. Respiration and ammonium excretion rates per unit mass of zooplankton size classes and
1017 taxa in Kongsfjorden, Svalbard, Barents and Greenland Sea, and Bransfield Strait, Southern
1018 Ocean. Values are means ± 1SD with number of measurements in parentheses.

Taxon	Month	Temp. (^{o}C)	Respiration (μg C mg C^{-1} h^{-}	Excretion (μg N mg C^{-1} h^{-}	Source
Thysanoessa spp.	Jan	2.5	0.49 ± 0.21 (22)	0.03 ± 0.01 (14)	0
	Apr	4	0.58 ± 0.10 (8)	0.07 ± 0.02 (8)	6
	May	2.5	0.48 ± 0.09 (6)	--	0
	May	0.1	0.76 ± 0.26 (11)	0.02 ± 0.01 (11)	4
	May	1.9	0.43 ± 0.12 (8)	0.04 ± 0.01 (8)	4
	Aug	4	0.58 ± 0.14 (8)	0.06 ± 0.03 (8)	6
	Sep	2.5	0.51 ± 0.21 (17)	0.06 ± 0.03 (14)	0
Mesozooplankton (>1000 μm)	Jan	2.5	2.66 ± 0.84 (6)	0.78 ± 0.32 (6)	0
	May	1-2.5	1.64 ± 0.21 (12)	--	0
	Sep	2.5	1.56 ± 0.35 (15)	1.09 ± 0.76 (9)	0
	Dec*	0-2.3	2.45 ± 1.56 (20)	0.38 ± 0.16 (20)	1
Mesozooplankton (200-1000 μm)	Jan	2.5	2.85 ± 0.39 (6)	0.55 ± 0.11 (6)	0
	May	1-2.5	2.28 ± 0.5 (12)	--	0
	Sep	2.5	1.72 ± 0.34 (15)	0.67 ± 0.11 (9)	0
	Dec*	0-2.3	2.27 ± 1.74 (3)	0.17 ± 0.12 (3)	1
Mesozooplankton (mixed; >200 μm)	Feb	-1.7	0.60 ± 0.24 (4)	--	2
	May	-1.7	0,47 ± 0.12 (4)	--	2
	Julw	-1.3-6.6	0.81 ± 0.46 (19)	0.22 ± 0.15 (19)	3
	Jul□	6.6	1.83 ± 0.19 (4)	0.68 ± 0.31 (4)	3
	Sep	-1	0.55 ± 0.12 (3)	--	2
Parasagitta elegans	May	-0.3	0.40 ± 0.10 (12)	0.15 ± 0.12 (12)	4
Themisto abyssorum	Jan	2.5	1.08 ± 0.17 (8)	0.26 ± 0.01 (5)	0
	Apr	1-2.5	0.36 ± 0.11 (6)	--	0
	May	1-2.5	0.50 ± 0.26 (3)	--	0
	Sep	2.5	0.66 ± 0.10 (4)	0.07 ± 0.01 (4)	0
Themisto libellula	Jan	2.5	0.76 ± 0.14 (7)	0.16 ± 0.03 (2)	0
	Apr	1-2.5	0.18 ± 0.01 (3)	--	0
	May	1-2.5	1.72 ± 0.28 (7)	--	0
	May	-0.1	0.92 ± 0.23 (11)	0.03 ± 0.01 (11)	4
	Aug	0	0.55 ± 0.18 (25)	--	5
	Sep	2.5	0.39 ± 0.17 (8)	0.02 ± 0.01 (3)	0

1019 (0) This study; (1) Hernández-León et al. (1999), * December corresponds to summer at the
1020 Antarctic peninsula; (2) Welch et al (1997); (3) Alcaraz et al. (2010), wmean of all
1021 measurements, □highest value measured during study; (4) Ikeda and Skjoldal (1989); (5) Auel
1022 and Werner (2003); (6) Huenerlage et al (2015).

1023 Table 3. Monthly average (± 1 SD) of euphausiids, copepods and chaetognaths daily respiration

1024 in, and export of carbon from the 40 and 82 m top layers in Kongsfjorden in 2014.

1025

Month	Respiration (mg C m^{-2} d^{-1})		Respiratory transport (mg C m^{-2} d^{-1})	
	2-40 m	2-82 m	Below 40 m	Below 82 m
	Euphausiids	Euphausiids	Euphausiids	Euphausiids
Jan	8.6 ± 7.2	19.1 ± 15.5	1.3 ± 1.0	-
Feb	7.7 ± 7.0	21.7 ± 23.2	3.5 ± 2.0	05.1 ± 2.6
Mar	4.1 ± 5.9	15.9 ± 23.4	4.6 ± 3.1	13.3 ± 5.9
Apr	1.8 ± 4.5	07.7 ± 24.6	1.0 ± 0.2	06.4 ± 9.3
May	7.1 ± 16.0	15.4 ± 35.6	-	-
Jun	5.8 ± 7.8	38.3 ± 46.7	-	-
Jul	2.6 ± 9.5	19.7 ± 36.7	-	-
Aug	1.1 ± 4.0	03.8 ± 13.0	2.4 ± 4.3	04.9 ± 5.7
Sep	1.2 ± 3.0	03.5 ± 09.1	2.1 ± 2.1	05.2 ± 4.3
	Copepods	Copepods	Copepods	Copepods
Jan	07.7 ± 3.1	15.9 ± 14.4	-	-
Feb	09.0 ± 3.4	20.0 ± 17.5	-	0.8 ± 3.2
Mar	08.8 ± 5.0	17.6 ± 15.9	0.9 ± 1.0	5.1 ± 6.8
Apr	09.7 ± 3.2	13.1 ± 09.9	1.0 ± 0.3	5.3 ± 8.2
May	10.5 ± 5.9	15.7 ± 16.8	-	-
Jun	13.8 ± 9.1	43.3 ± 43.0	-	-
Jul	13.3 ± 39.3	17.5 ± 12.8	-	-
Aug	09.0 ± 3.1	10.5 ± 05.1	0.3 ± 0.6	1.1 ± 6.2
Sep	08.3 ± 2.0	09.8 ± 04.0	0.3 ± 0.3	1.4 ± 7.2
	Chaetognaths	Chaetognaths	Chaetognaths	Chaetognaths
Jan	0.4 ± 0.3	1.0 ± 0.8	0.1 ± 0.0	
Feb	0.4 ± 0.4	1.2 ± 1.3	0.2 ± 0.1	0.3 ± 0.2
Mar	0.2 ± 0.3	0.8 ± 1.1	0.2 ± 0.1	0.7 ± 0.2
Apr	0.1 ± 0.3	0.4 ± 1.3	<0.1	0.4 ± 0.4
May	0.4 ± 1.1	0.9 ± 2.3	-	-
Jun	0.3 ± 0.5	2.1 ± 2.6	-	-
Jul	0.2 ± 2.1	1.2 ± 4.4	-	-
Aug	0.1 ± 0.2	0.2 ± 0.6	0.1 ± 0.3	0.2 ± 0.1
Sep	0.1 ± 0.2	0.2 ± 0.5	0.1 ± 0.1	0.3 ± 0.3

1026

1027 Table 4. Monthly average (± 1SD) of euphausiids, copepods and chaetognaths daily excretion in,

1028 and export of nitrogen from the 40 and 82 m top layers in Kongsfjorden in 2014.

Month	Excretion (mg N m^{-2} d^{-1})		Excretory transport (mg N m^{-2} d^{-1})	
	0-40 m	0-80 m	Below 40 m	Below 80 m
	Euphausiids	Euphausiids	Euphausiids	Euphausiids
Jan	0.53 ± 0.45	1.19 ± 0.96	0.08 ± 0.06	-
Feb	0.48 ± 0.43	1.35 ± 1.44	0.22 ± 0.13	0.32 ± 0.16
Mar	0.25 ± 0.37	0.99 ± 1.46	0.28 ± 0.19	0.83 ± 0.36
Apr	0.11 ± 0.28	0.48 ± 1.53	0.06 ± 0.01	0.40 ± 0.58
May	0.86 ± 1.94	1.87 ± 4.31	-	-
Jun	0.70 ± 0.94	4.63 ± 5.64	-	-
Jul	0.31 ± 1.15	2.39 ± 4.44	-	-
Aug	0.13 ± 0.48	0.46 ± 1.57	0.29 ± 0.52	0.60 ± 0.68
Sep	0.15 ± 0.37	0.43 ± 1.10	0.25 ± 0.25	0.63 ± 0.52
	Copepods	Copepods	Copepods	Copepods
Jan	4.28 ± 1.73	08.79 ± 8.00	-	-
Feb	4.99 ± 1.87	11.08 ± 9.72	-	0.43 ± 1.78
Mar	4.88 ± 2.75	09.73 ± 8.79	0.48 ± 0.53	2.83 ± 3.78
Apr	5.35 ± 1.76	07.24 ± 5.51	0.53 ± 0.16	2.93 ± 4.53
May	5.81 ± 3.26	08.71 ± 9.31	-	-
Jun	7.65 ± 5.07	23.97 ± 23.82	-	-
Jul	7.35 ± 21.77	09.68 ± 7.08	-	-
Aug	4.97 ± 1.73	05.82 ± 2.85	0.15 ± 0.34	0.61 ± 3.41
Sep	4.62 ± 1.12	05.45 ± 2.24	0.14 ± 0.18	0.78 ± 3.99
	Chaetognaths	Chaetognaths	Chaetognaths	Chaetognaths
Jan	0.15 ± 0.12	0.37 ± 0.32	0.02 ± 0.02	-
Feb	0.15 ± 0.14	0.45 ± 0.50	0.07 ± 0.03	0.10 ± 0.06
Mar	0.07 ± 0.10	0.32 ± 0.43	0.08 ± 0.04	0.28 ± 0.08
Apr	0.04 ± 0.12	0.16 ± 0.49	0.02 ± 0.00	0.15 ± 0.17
May	0.16 ± 0.41	0.36 ± 0.88	-	-
Jun	0.12 ± 0.18	0.80 ± 0.97	-	-
Jul	0.06 ± 0.81	0.44 ± 1.67	-	-
Aug	0.02 ± 0.07	0.07 ± 0.23	0.05 ± 0.12	0.09± 0.05
Sep	0.02 ± 0.06	0.07 ± 0.19	0.04 ± 0.05	0.12 ± 0.13

1029

1030

1031

Supplemental Table S1. Specifications of the AZFP at each frequency used in the study.

Frequency (kHz)	Vertical resolution (cm)	Nominal Source Level (dB re 1µPa at 1m)	Nominal -3dB beam angle (º)	Pulse duration (ms)
125	98.4	210	8	3
200	47.2	210	8	3
455	23.6	210	7	1.5

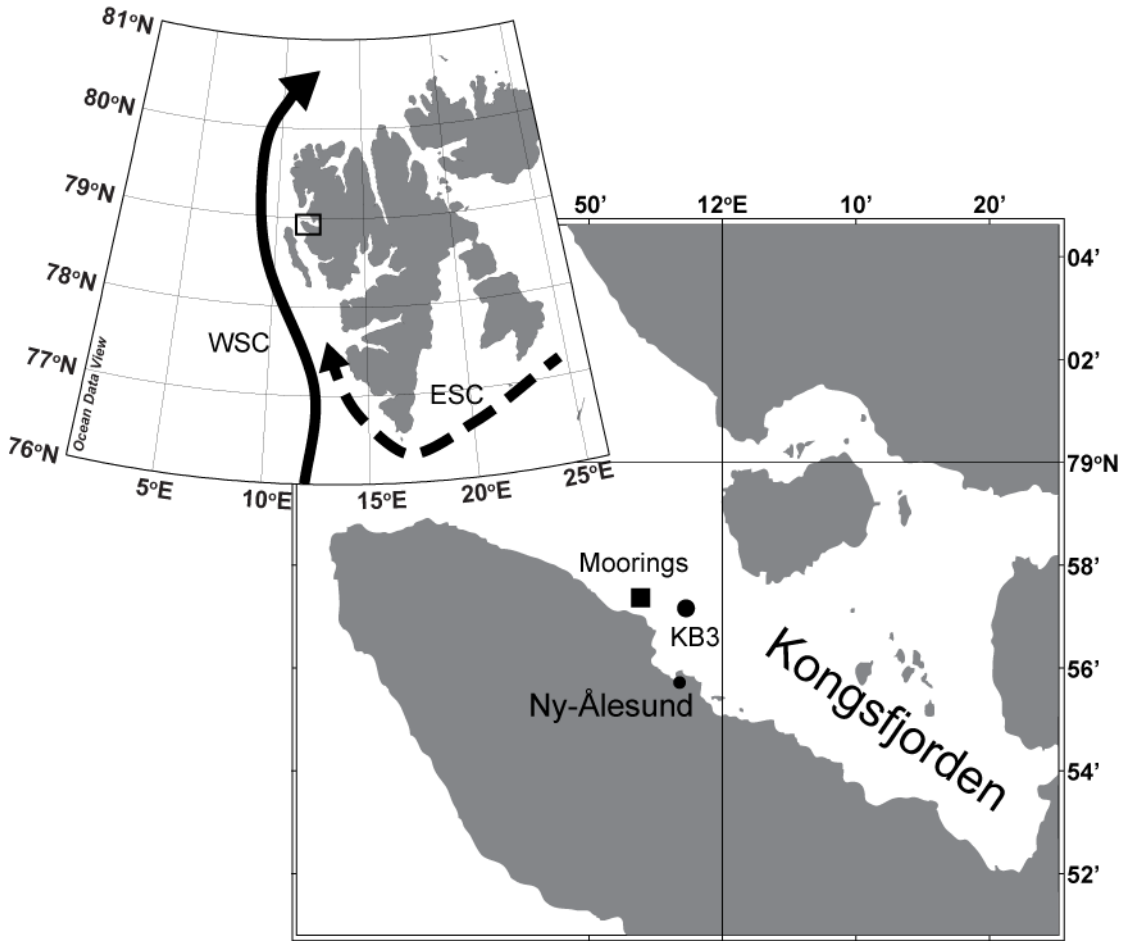

Fig. 1. Location of the sampling station KB3 in Kongsfjorden and of three moorings; one with an Acoustic Zooplankton Fish Profiler, one with two Acoustic Doppler Current Profilers, and another with fluorescence and PAR sensors (Table 1) The northward flowing West Spitsbergen Current (WSC; black arrow) and East Spitsbergen Current (ESC; dashed arrow) are illustrated.

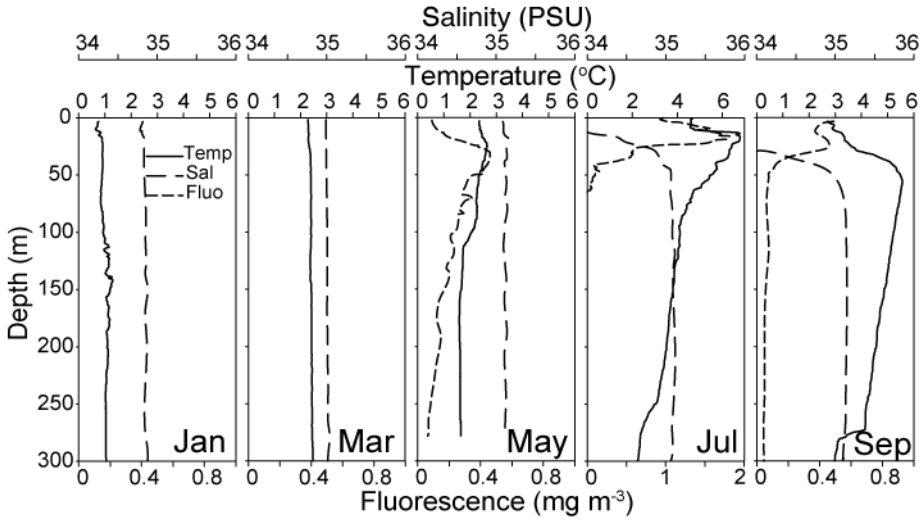

Fig. 2. Vertical profiles of temperature, salinity and fluorescence at station KB3 in Kongsfjorden at different dates of 2014.

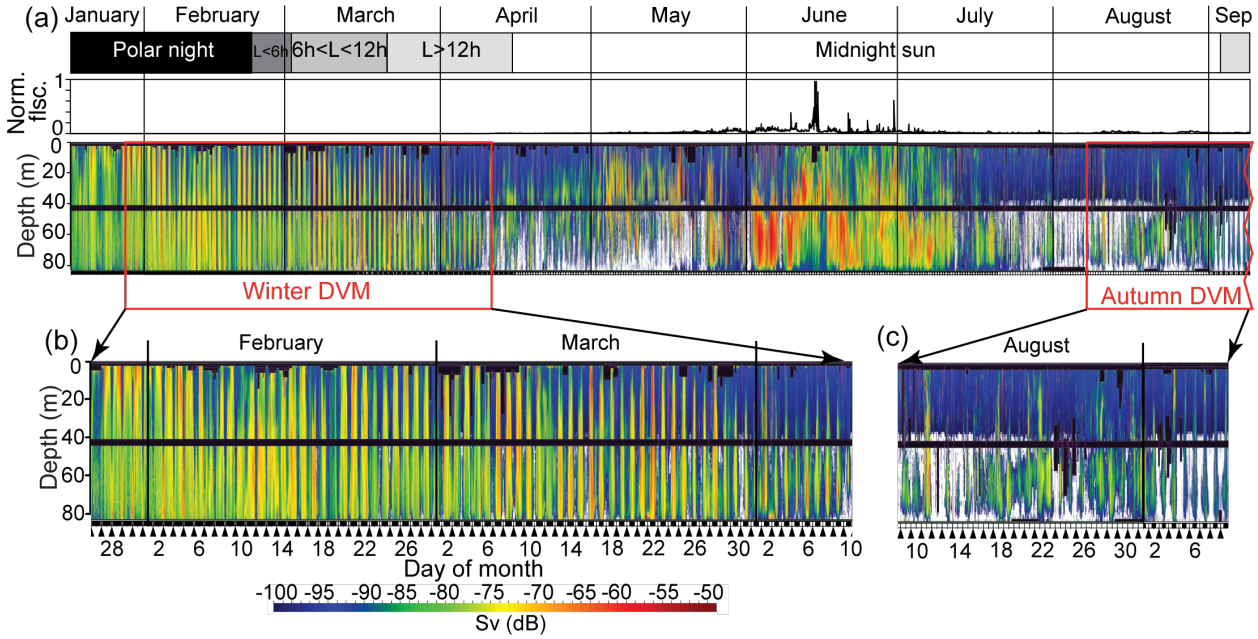

Fig. 3 (a) Time series of relative fluorescence (Norm. flsc.) at 37 m depth and backscatter for the 125 kHz frequency of the AZFP in Kongsfjorden from 17 January to 9 September 2014, and expanded views of (a) winter DVM period (28-January-10 April) and (c) onset of autumn DVM (10 August-9 September) defined qualitatively by visual analysis of the echogram.

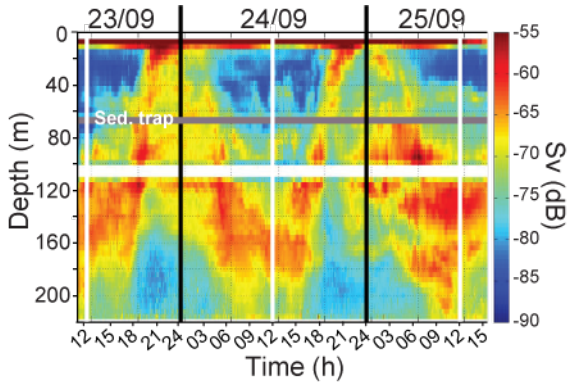

Fig. 4. Backscatter from two 307.2 kHz ADCPs, one upward-looking and the other downward-looking, from 23 to 25 September 2014 at the mooring site. Black and white vertical lines indicate local midnights and middays as per the clock.

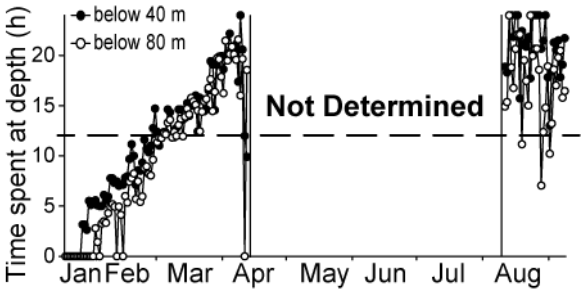

Fig. 5. Time series of time spent below 40 and 80 m depth by the high backscatter over a 24-h cycle from January to September 2014. The horizontal broken line indicates the 12-h limit.

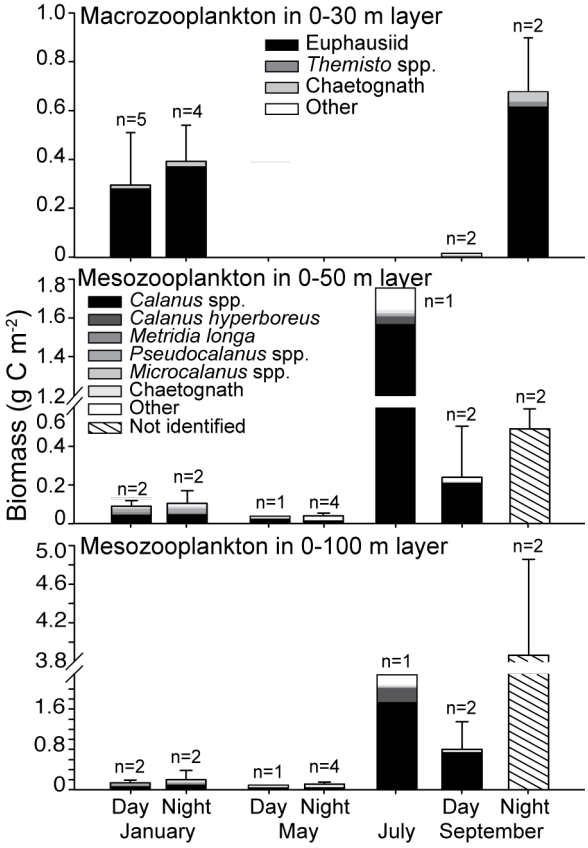

Fig. 6. Macro- and mesozooplankton biomass and composition from plankton net data in the surface 30, 50 and 100-m layer at day and at night in January, May, July and September 2014 at station KB3 in Kongsfjorden. “n” indicates number of plankton net deployments.

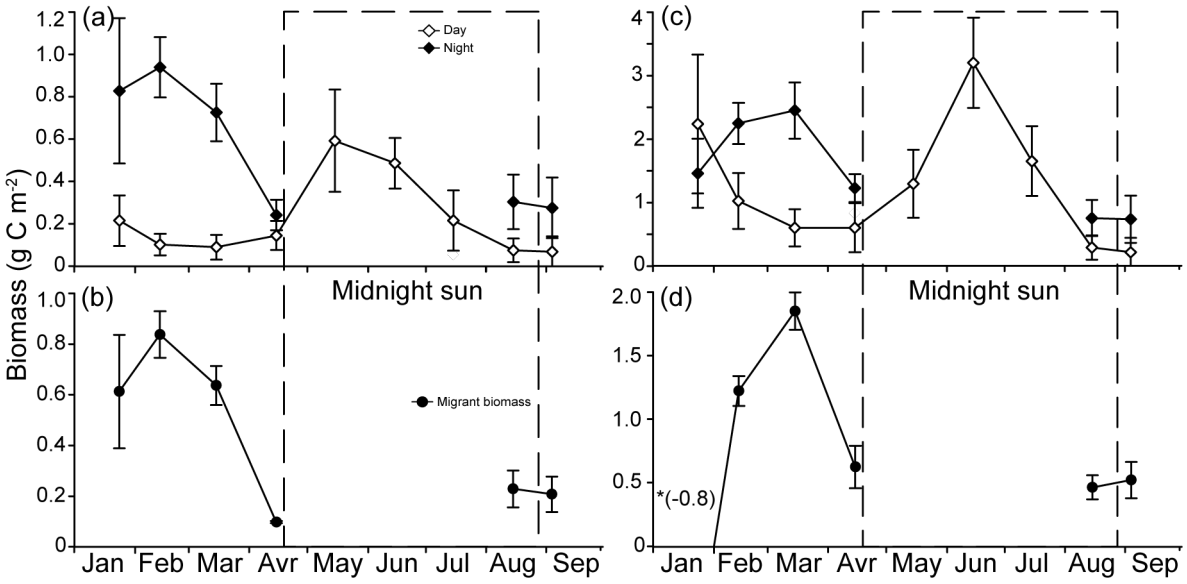

Fig. 7. Euphausiids. (a and c) time series of average monthly day and night biomass (± 1 SE) in the 40 m and 80 m above the AZFP, respectively, and (b and d) respective diel migrant biomass (± 1 SE) in the same layers, with *negative value indicating biomass during day higher than night. Note different scales on the y-axis among panels.

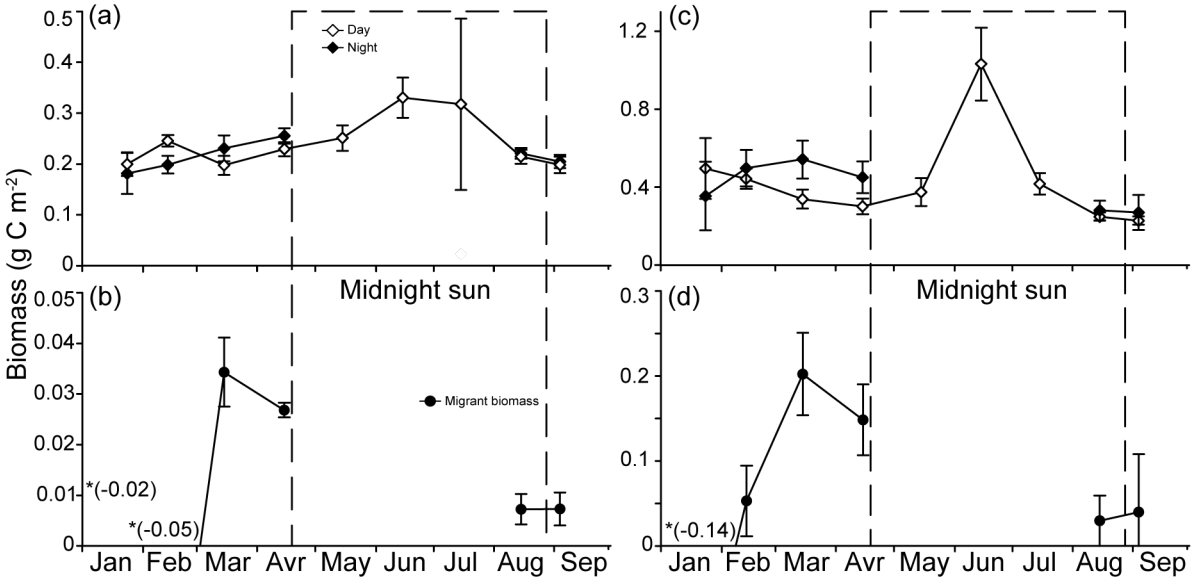

Fig. 8. Copepods. (a and c) time series of average monthly day and night biomass (± 1 SE) in the 40 m and 80 m above the AZFP, respectively, and (b and d) respective diel migrant biomass (± 1 SE) in the same layers, with *negative value indicating biomass during day higher than night. Note different scales on the y-axis among panels.

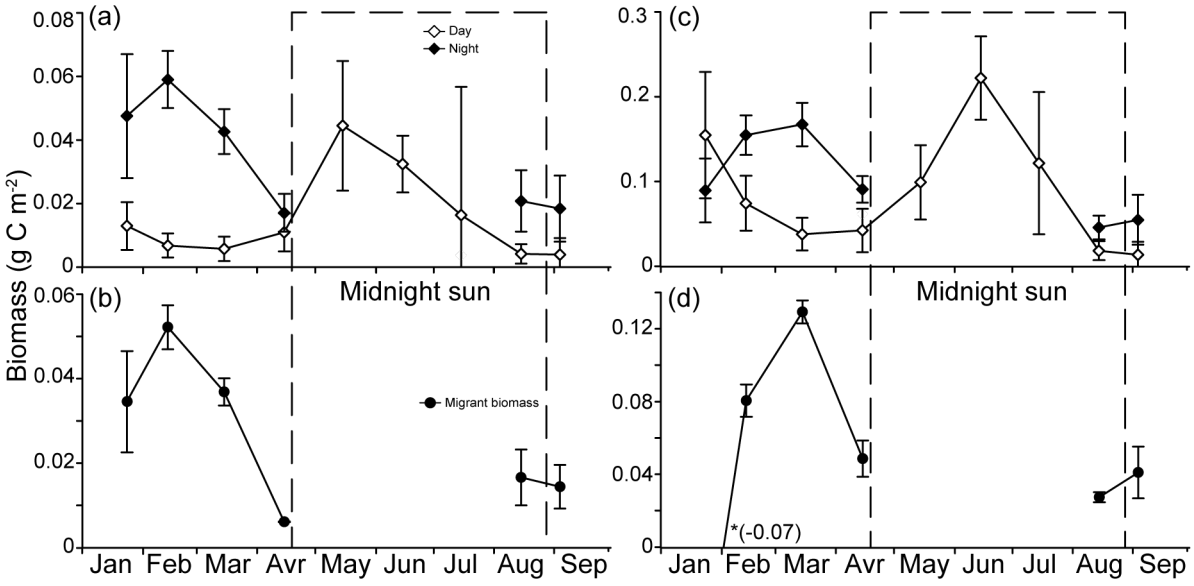

Fig. 9. Chaetognaths. (a and c) time series of average monthly day and night biomass (± 1 SE) in the 40 m and 80 m above the AZFP, respectively, and (b and d) respective diel migrant biomass (± 1 SE) in the same layers, with *negative value indicating biomass during day higher than night. Note different scales on the y-axis among panels.

Supplemental information

Table S1. Specifications of the AZFP at each frequency

Frequency (kHz)	Vertical resolution (cm)	Nominal Source Level (dB re 1µPa at 1m)	Nominal -3dB beam angle (º)	Pulse duration (ms)
125	98.4	210	8	3
200	47.2	210	8	3
455	23.6	210	7	1.5

Table S2. Parameters used to calculate mean TS and biomass of each zooplankton group based on the randomly oriented fluid bent-cylinder model (Stanton et al. 1994)

Taxon	R reflection coeff.	L mean body length (m)	s standard deviation of length·length^{-1}	β_D body length to width ratio	D body width (m)	f acoustic freq. (Hz)	c sound speed (m s^{-1})	TS (dB re 1m^{-2})	W mean dry weight (mg)
Euphausiid	0.058[a]	0.015[c]	0.261[c]	8.8[d]	0.002[c]	125 000	1500	-84.52	17.979[e]
Copepod	0.038[b]	0.00236[c]	0.152[c]	2.72[d]	0.001[c]	455 000	1500	-93.79	0.205[e]
Chaetognath	0.030[b]	0.018[d]	0.0277[d]	18.7[d]	0.001[d]	200 000	1500	-93.96	0.894[f]

[a]Kristensen and Dalen (1986); [b]Lawson et al. (2004); [c]Measured from net samples; [d]Berge et al. (2014), [e]Dry weight measurements (unpublished data); [f]Welch et al. (1996)

Table S3. Estimates of zooplankton diel migrant biomass and active carbon respiratory flux (± 1 SD and range between brackets) due to DVM in different oceanic regions. Meso and Macro referring to the meso- and macro-zooplankton size classes, respectively.

Region	Time of year	Component	Migrant biomass (mg C m^{-2})	Respiratory flux (mg C m^{-2} d^{-1})	% of POC flux	Depth (m)	Source
Subtropic. Atlantic	Sep	Meso+Macro	47-148	2.8-8.8	4-14	150	1
	Sep	Meso+Macro	51-1797	21-431	13-58	Pyc*	1
Bermuda (BATS)	Mar-Apr	Meso	192 (84-540)	14.5 (6.2-14.8)	18-70	150	2
	All year	Meso+Macro	50 (0-123)	2.0 (0-9.9)	0-39	150	3
Canary Islands	Aug	Meso	125-248	1.9-4.3	22-28	150	4
	Jun	Meso	580-1280	1.9-8.3	15-53	200	5
	Mar	Meso	108-341	0.5-1.4	1-3	200	6
North Atlantic	Oct-Nov	Meso	360 ± 70	30.3 ± 1.9	-	200	7
Equat. Pacific	Mar-Apr	Meso	96 ± 25	4 ± 1	18	150	8
	Sep-Oct	Meso	155 ± 32	7 ± 1	25	150	8
	Sep-Oct	Meso	47	3	8	150	9
	Sep-Oct	Meso	-	-	4	150	10
	Feb	Meso	367 (145-446)	13.2 (7.3-19.1)		160	11
Subtropic. Pacific	All year	Meso+Macro	162 (108-216)	3.6 (2.6-4.8)	12-18	150	12
	Jun-Jul	Meso+Macro	137	3.7	18	150	13
California current	Apr-Oct	Meso+Macro		2.4-47.1	2-41	100	14
North Pacific	Aug	*Metridia* sp.	59-1676	1-15.8	15	150	15
Subarctic Pacific	All year	*Metridia* sp.	116	3	10	150	16
		Meso+Macro	1350	12-35	18	150	13
High Arctic	Jan	Meso+Macro	629 ± 506	1.3 ± 1.2	1.1	50	17
(Kongsfjorden)	Feb	Meso+Macro	844 ± 544	3.0 ± 2.5	2.6	50	17
	Mar	Meso+Macro	708 ± 486	5.7 ± 4.1	4.8	50	17
	Apr	Meso+Macro	130 ± 31	2.0 ± 0.5	1.7	50	17
	Aug	Meso+Macro	252 ± 423	2.8 ± 3.6	2.4	50	17
	Sep	Meso+Macro	229 ± 215	2.5 ± 1.8	2.1	50	17
	Feb	Meso+Macro	1356 ± 447	6.2 ± 0.6	3.8	100	17
	Mar	Meso+Macro	2182 ± 1119	19.2 ± 12.7	11.8	100	17
	Apr	Meso+Macro	823 ± 738	12.1 ± 1.1	7.4	100	17
	Aug	Meso+Macro	522 ± 715	6.3 ± 0.5	3.8	100	17
	Sep	Meso+Macro	603 ± 674	7.0 ± 11.5	4.3	100	17

(1) Longhurst et al. (1990); (2) Dam et al. (1995); (3) Steinberg et al (2000); (4) Hernández-León et al. (2001); (5) Yebra et al. (2005); (6) Putzeys et al. (2011); (7) Isla and Anadón (2004); (8) Zhang and Dam (1997); (9) Le Borgne and Rodier (1997); (10) Rodier and Le Borgne (1997); (11) Hidaka et al. (2001); (12) Al Mutairi and Landry (2001); (13) Steinberg et al (2008); (14) Stukel et al. (2013); (15) Takahashi et al. (2009); (16) Kobari et al. (2008); (17) This study. *Pyc. referring to depth of the pycnocline (47-200 m).

Table S4. Estimates of zooplankton active nitrogen excretory flux (± 1 SD and range between brackets) due to DVM in different oceanic regions. Meso and Macro referring to the meso- and macro-zooplankton size classes, respectively.

Region	Time of year	Component	Excretory flux (mg N m^{-2} d^{-1})	% of PON flux	Depth (m)	Source
Sargasso Sea	Sep	Meso	0.72	7.7	100	1
(BATS)	Sep	Meso+Macro	0.4	8.7	150	2
	Mar-Apr	Meso	1.9 (0.8-8.3)	17-82	150	3
Equat. Pacific:						
Oligotrophic	Sep-Oct	Meso+Macro	3.6	45	150	4, 5
HNLC area	Sep-Oct	Meso+Macro	3.6	9	150	4, 5
Tropic. Pacific	All year	Meso+Macro	0.4	8	60	6
	Apr	Meso+Macro	2.9	23.9	55	6
	Apr	Meso+Macro	1.7	2.5	35	6
	All year	Meso+Macro	0.6 (0.2-1.6)	7-35	150	7
Panama Basin	Aug	Meso+Macro	2.3	34.9	70	6
	Nov	Meso+Macro	1.2	26.4	70	6
North Pacific gyre	Aug	Meso+Macro	0.8	60.9	130	6
	Aug	Meso+Macro	2.5	107.6	112	6
Indian Ocean	Mar-Jun	Meso+Macro	1.8	25.9	90	6
	Mar-Jun	Meso+Macro	1.1	10.1	50	6
Celtic Sea	Aug	Meso+Macro	16.5	56.8	30	6
High Arctic	Jan	Meso+Macro	0.1 ± 0.1	0.6	50	8
(Kongsfjorden)	Feb	Meso+Macro	0.3 ± 0.2	1.7	50	8
	Mar	Meso+Macro	0.8 ± 0.8	5.0	50	8
	Apr	Meso+Macro	0.6 ± 0.2	3.6	50	8
	Aug	Meso+Macro	0.5 ± 0.3	2.9	50	8
	Sep	Meso+Macro	0.4 ± 0.1	2.6	50	8
	Feb	Meso+Macro	0.9 ± 1.6	4.0	100	8
	Mar	Meso+Macro	3.9 ± 4.2	18.3	100	8
	Apr	Meso+Macro	3.5 ± 3.8	16.2	100	8
	Aug	Meso+Macro	1.3 ± 4.1	6.0	100	8
	Sep	Meso+Macro	1.5 ± 4.6	7.1	100	8

(1) Longhurst et al. (1989); (2) Steinberg et al (2002); (3) Dam et al. (1995); (4) Le Borgne and Rodier (1997); (5) Rodier and Le Borgne (1997); (6) Longhurst and Harrison (1988); (7) Al Mutairi and Landry (2001); (8) This study.

Table S5. Zooplankton particulate organic carbon and nitrogen (POC and PON) sinking flux at the depths of sediment traps in 2012 in Adventfjorden and Kongsfjorden.

Month	Fjord	Condition	Depth (m)	POC flux (mg C m^{-2} d^{-1})	PON flux (mg N m^{-2} d^{-1})	Source
May	Kongsfjorden	Bloom	50	542	60	1
			100	844	104	1
Aug	Kongsfjorden	Post-bloom	50	128	17	1
			100	229	27	1
Oct	Kongsfjorden	Post-bloom	50	104	17	1
			100	105	16	1

(1) Lalande et al. (2016) only for POC flux; PON flux in Kongsfjorden from unpublished data.

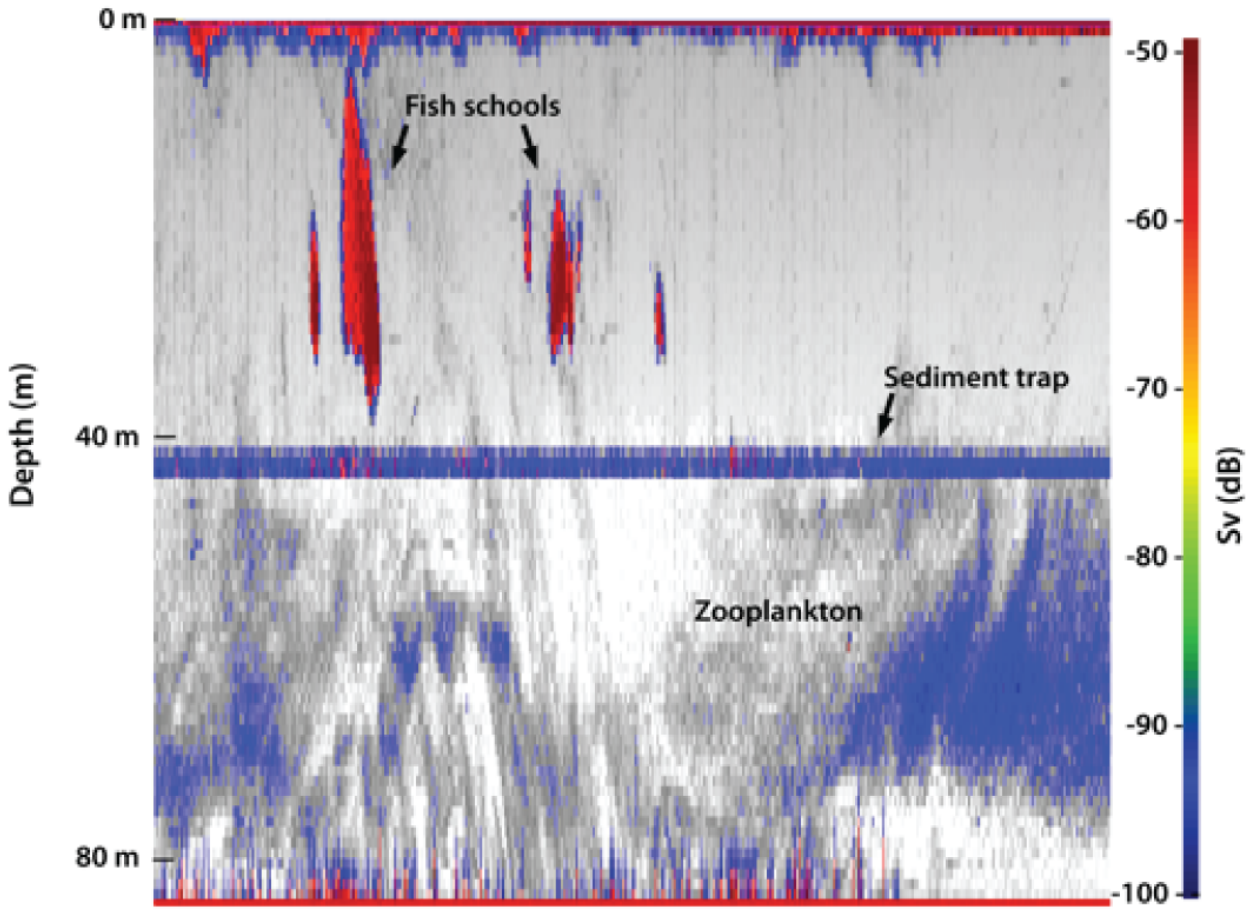

Fig. S1. Example of a 125-kHz echogram with backscatters from fish schools and zooplankton.

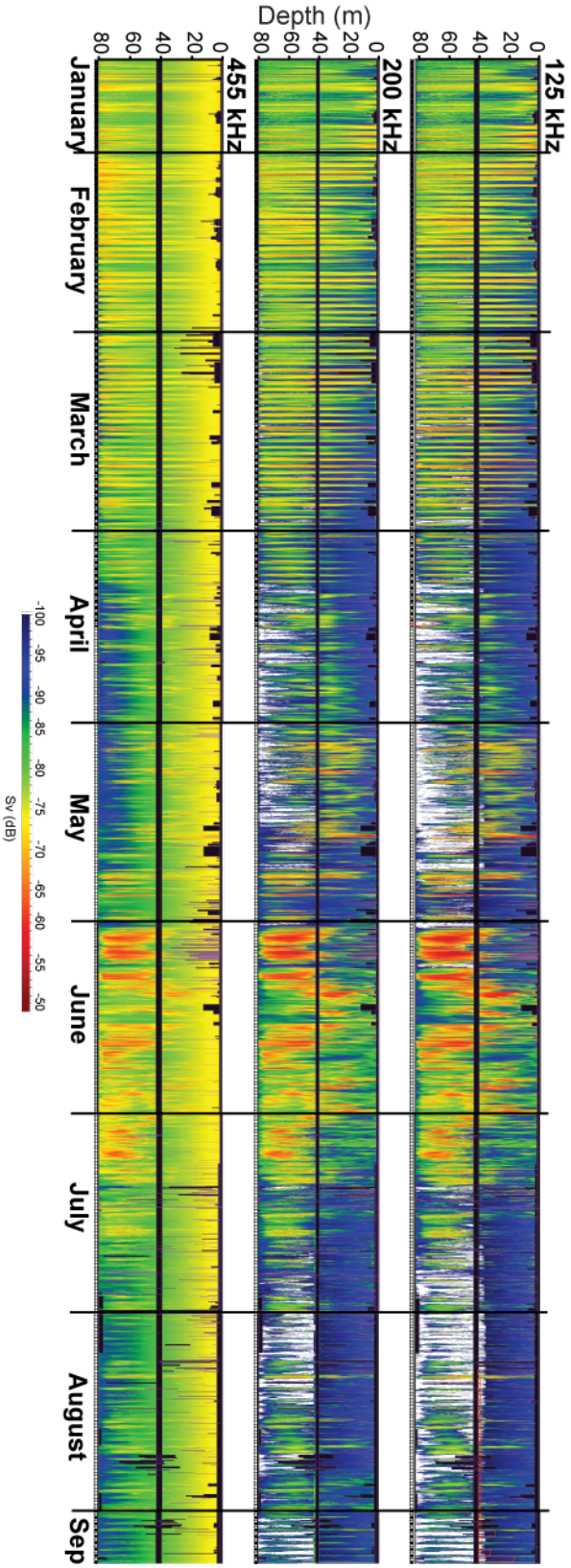
Depth (m)
125 kHz
200 kHz
455 kHz
January
February
March
April
May
June
July
August
Sep
Sv (dB)

1153
1154

Fig. S2. Echograms at 125, 200 and 455 kHz of the AZFP in Kongsfjorden from 17 January to 9 September 2014.